2021

Coastal Setting Determines Tidal Marsh Sustainability with Accelerating Sea-level Rise

Karinna Nunez
Virginia Institute of Marine Science

Yinglong J. Zhang
Virginia Institute of Marine Science

Donna M. Bilkovic
Virginia Institute of Marine Science

Carl Hershner
Virginia Institute of Marine Science

Recommended Citation

Nunez, Karinna; Zhang, Yinglong J.; Bilkovic, Donna M.; and Hershner, Carl, Coastal Setting Determines Tidal Marsh Sustainability with Accelerating Sea-level Rise (2021). *Ocean & Coastal Management*, 214, 105898.
doi: 10.1016/j.ocecoaman.2021.105898

Coastal Setting Determines Tidal Marsh Sustainability with Accelerating Sea-level Rise

Karinna Nunez[a], Yinglong J. Zhang[a], Donna M. Bilkovic[a], Carlton Hershner[a]

[a] Virginia Institute of Marine Science, William & Mary. P.O. Box 1346, Gloucester Point, Virginia, USA.

Corresponding author: Karinna Nunez
e-mail: karinna@vims.edu
phone: (804) 684-7273
fax: (804) 684-7179.

HIGHLIGHTS:

- Enhanced TMM advances the understanding of sea-level rise impacts on tidal marshes
- TMM accounts for geomorphology, sediment supply, vegetation, and human factors
- TMM elucidates the effects of coastal settings on the evolution of tidal marshes

Abstract

There is an increasing concern over how accelerated rates of sea-level rise (SLR) will impact tidal marsh ecosystems. The present study evaluates the potential impacts of SLR on marsh sustainability using the Tidal Marsh Model (TMM) with the addition of a new vegetation algorithm within the SCHISM (Semi-implicit Cross-scale Hydroscience Integrated System Model) framework. This new functionality contributes to an improved understanding of how vegetation affects the mean flow velocity and turbulence, and consequently, the sedimentation processes. Using two SLR scenarios (intermediate and extreme SLR rates), we projected the changes in marsh extent over the next 50 years in two representative marsh systems within a subestuary of Chesapeake Bay. Each study site has marshes associated with different physical settings and anthropogenic components: Carter Creek (developed, high topography) vs. Taskinas Creek (natural, low topography, steep banks). Carter Creek experienced a net marsh loss of 7.3% and 60% in the intermediate and extreme SLR scenario, respectively. In some places, due to the local geomorphic settings, marshes were able to migrate inland and offset part of the total loss, whereas marsh transgression was truncated near development and hardened shoreline structures. In Taskinas Creek, marshes are associated with natural lands with steep upland slopes (inhibitor for marsh transgression due to SLR). Marsh net decline was 23.1% (intermediate SLR scenario), and 89.6% (extreme SLR scenario). Marsh transgression was not substantial in this site, suggesting that marsh loss can be primarily attributed to upland bank conditions which prevented marsh migration with accelerated SLR rates. The enhanced TMM provides the highly-resolved simulations of multi-scale processes needed to inform restoration, strategic planning, and monitoring activities to support marsh sustainability in an evolving system.

Keywords: marshes, tidal marsh model, sea-level rise, cross-scale simulation, SCHISM

1. Introduction

Tidal marshes are among the most valuable ecosystems in terms of productivity and species diversity. They provide many ecosystem services including shoreline stabilization, water quality improvements, habitat for many organisms, and long-term carbon storage (Allen 2000; Fagherazzi et al. 2004; Zedler and Kercher 2005; Barbier et al. 2011). Tidal marshes occur in a broad range of geomorphic settings with different hydrodynamics, sediment sources, and vegetative communities (Titus et al. 2009). Their establishment and persistence are influenced by environmental factors (e.g., temperature, salinity), different landscapes, coastal processes, as well as anthropogenic activities (e.g., nearshore development, shoreline armoring) (Zhu et al. 2014; Fagherazzi et al. 2019). Geomorphological processes are responsible for shaping the physical structure of marshes, thus influencing movement of water, sediments, and nutrients (Leonardi and Fagherazzi 2014). These physical processes provide the framework where marsh ecological processes take place.

Marsh habitats have the capacity to dynamically change in response to environmental conditions. Climate change drivers will have different effects on tidal marshes. Changes in tidal regimes, storm patterns, sea-level rise (SLR), as well as human activities that respond to climate change will affect marsh ecosystems and influence their future extent and distribution (Raposa et al. 2017; Horton et al. 2018). There is a universal consensus that global sea levels will rise at an increased rate from those in the recent past (Cazenave and Nerem 2004; Rahmstorf 2007; Boon and Mitchell 2015). Rising seas will increase the vulnerability of coastal communities and ecosystems, and as a result, the supporting services they provide (Parris et al. 2012; Hall et al. 2016).

It is well established that marsh elevation changes in response to SLR (Cahoon and Guntenspergen 2010; Kolker et al. 2010). These habitats have the capacity to adapt to inundations associated with rising sea level by two mechanisms: vertical accretion and horizontal migration (Morris et al. 2002; Kirwan and Murphy 2007; Raposa et al. 2017; Horton et al. 2018). A tidal marsh will be able to persist in the same location if it builds vertically at a rate equal or higher than the rise in sea level (Reed 1995). If the sea level rises faster than the marsh elevation builds vertically, then the marsh will become submerged.

Tidal marshes accrete vertically through the deposition of mineral sediments and organic matter accumulation (Morris et al 2002; Fagherazzi et al. 2012). Inorganic sediment sources to the marsh include bank erosion, sediments coming from upland runoff, and tidally delivered sediments. Mineral sediments are deposited on the marsh surface when the marsh is flooded. The inorganic suspended sediment transport and deposition on marshes will be determined by rates of particle settling, tidal range and inundation depth, and vegetation density. These parameters vary spatially; and for that reason, sediment accretion rates will vary depending on the different vegetative communities and the geomorphic settings (Titus et al. 2009).

Marshes also have the capacity to respond to SLR conditions by moving horizontally to higher elevations, either to adjacent land or into adjacent waters if they are filled with sediment. In order for the marshes to migrate inland, they need to have an adjacent open space that allows transgression. This natural response of marshes is truncated in many cases due to increased coastal development which utilizes hardened shoreline structures to stabilize the shoreline and protect public lands and private properties from erosion (Titus et al. 2009; Gittman et al. 2015; Hill 2015; Enwright et al. 2016).

Marsh plants play an important role in nearshore hydrodynamics (i.e., waves, current velocity and direction, and water levels) in creeks, rivers, estuaries, and coastal regions (Temmerman et al. 2005; D'Alpaos et al. 2007a; Kiss and Jozsa 2014). The interactions between coastal vegetation and nearshore hydrodynamics have been the focus of many studies (e.g., Gedan et al. 2011; Shepard et al. 2011; Spalding et al. 2014; Sutton-Grier et al. 2015). Coastal marshes have the ability to modify the circulation pattern by being an obstacle to water motion, affecting the mean flow velocity and turbulence, as well as attenuating wave energy by reducing wave heights entering them (Roland and Douglass 2005; Leonard and Croft 2006; Costanza et al. 2008; Feagin et al. 2009; Gedan et al. 2011; Anderson and Smith 2014; Marsooli and Wu 2014; John et al. 2015). Correlation between plant density and sediment deposition rates (e.g., Morris et al. 2002; Li and Yang, 2009; Shepard et al. 2011; Ysebaert et al. 2011; Silliman et al. 2015) suggests that the greater the marsh density, the higher the concentration of suspended sediment trapped in the marsh field, and the more resilient the marsh will be to wave energy and SLR.

There is an increasing interest among resource managers and decision makers in spatially-explicit assessments of potential SLR impacts on tidal marshes. To that end, different models have been developed and applied to predict marsh spatial extent and future distribution (Morris et al. 2002; McLeod et al. 2010; Mogensen and Rogers, 2018; Alizad et al. 2018). Current models are constrained by the limitations of the two modeling approaches: landscape-scale models and site-specific models. For instance, landscape-scale models (e.g. Sea Level Affecting Marshes Model, SLAMM) use fixed rates during the entire simulation. They simulate general trends over large areas, but usually at a very coarse resolution. Thus, these types of models are not suitable for site-specific research and management uses because scaling down the results to local levels is not feasible, limiting their accuracy and effectiveness to local applications. On the contrary, site-specific models (e.g. Marsh Evolution Model, MEM) are more mechanistic. Several studies have applied site-specific models to evaluate the long-term evolution of marshes under the effect of SLR (e.g., Kirwan and Murray 2007; Mariotti and Fagherazzi, 2010; Alizad et al. 2016). They are applied to simulate responses for a specific site with a particular set of conditions and settings. One of the main limitations of these approaches is the extrapolation of model results to regional levels. Using results from an individual site to generate long-term projections at larger spatial extents is challenging due to the broad range of geomorphic settings across landscapes (Titus et al. 2009; Nunez 2020).

To address and overcome many limitations that current marsh models present, we expanded the capability of an existing multi-scale, hydrodynamic marsh evolution model (Tidal Marsh Model [TMM], Nunez et al. 2020) in order to increase our current knowledge of how marshes may respond to changes in sea level in different settings. The TMM has been developed within the SCHISM framework (Semi-implicit Cross-scale Hydroscience Integrated System Model) (Zhang et al. 2016), an open-source, next-generation hydrodynamic modeling system. Some of the unique features the TMM includes are cross-scale simulations, dynamic rates (i.e. rates vary in space and time as determined by changes in the hydrodynamic conditions of the system), semi-implicit time stepping method, and incorporation of anthropogenic stressors.

The present study has two main objectives. First, develop, test, and validate via hindcast a new model component in the TMM that captures the interactions between marsh vegetation and hydro/sediment dynamics. The incorporation of a new vegetation algorithm in the TMM will allow for a more accurate simulation of the water flow and turbulence within the marsh. Modeling the feedback between marsh plants and sediment processes allows simulation of the evolution of the tidal marsh platform, calculated with reference to the relative mean-sea level

(MSL). Second, apply the enhanced version of the TMM to evaluate the primary processes affecting marsh sustainability in different geomorphic settings over the next 50 years.

2. Materials and Methods

2.1 Study Area

The TMM with the new vegetation algorithm (hereafter TMM_VEG) was tested and applied in two tidal creeks within the York River estuary in the southern region of Chesapeake Bay, Virginia, USA (Figure 1a): Carter Creek (Figure 1b), and Taskinas Creek (Figure 1c). These two creeks were selected because they are characteristic of the western shore of the Chesapeake Bay, capturing the variation in geomorphic settings common in the region. In addition, these study areas were previously evaluated using the TMM without the vegetation algorithm (Nunez et al., 2020), which allowed for direct comparison of model outputs. Carter Creek is located on the northern side of the York River, approximately 22 km from the mouth of the river. Its watershed is characterized mainly by agricultural and residential land uses. Development pressure has resulted in the presence of roads and hardened shoreline structures in direct contact with marsh habitat. The upland bank height ranges between zero and 1.5 m relative to MSL (CCRM 2018), with gentle bank slope of less than 10 degrees (Danielson and Tyler 2016). The geomorphic marsh settings in this creek include fringe and embayed marshes. Fringe marshes have a much greater length than width and occur along sections of the shoreline. Embayed marshes are V-shaped marshes that form along the edges and upper reaches of creeks. The dominant marsh plant species (i.e., more than 50% of the marsh areal extent) in this system is *Spartina alterniflora* (CCRM 2018). The total marsh areal extent evaluated in this system was 594,888 m^2.

Taskinas Creek is located on the southern side of the York River, approximately 38 km from the mouth of the river. This is a very pristine environment; it is a component of the Chesapeake Bay National Estuarine Research Reserve (CBNERR). In most of this tidal system, the upland bank height is greater than 1.5 m relative to MSL (CCRM 2018), and mostly with a bank slope greater than 30 degrees (Danielson and Tyler 2016). This creek system is characterized by embayed marshes, which are primarily associated with forested and agricultural land uses. In this system, *S. alterniflora* is also the dominant plant species (CCRM 2018). The total marsh areal extent evaluated in this system was 481,576 m^2.

2.2 Tidal Marsh Model (TMM)

The TMM integrates the physical and anthropogenic components needed to simulate and assess the evolution and persistence of tidal marshes as sea level rises. The TMM simulates marsh migration under the combined influence of tides, wind waves, sediment transport, precipitation, riparian land use, shoreline armoring (e.g., bulkhead, riprap), and roads. The model assesses marsh edge changes as well as internal marsh changes due to variations in elevation and sediment supply, which can lead to internal marsh fragmentation.

The TMM is connected to three major modules in the SCHISM system: the hydrodynamic core that serves as the foundation of the SCHISM modeling system; the 3D sediment transport model (CSTMS); and the wind wave model (WWM-III) (Figure 2). WWM-III (Roland 2009; Roland et al. 2012) is a community-driven, parallel, and advanced numerical framework that can be applied to study wave-current interaction processes based on unstructured grids. CSTMS is an adaptation from Warner et al. (2008).

Unlike existing marsh models (e.g., Clough et al. 2010; Odink 2019), the TMM uses an unstructured grid in the simulations, which allows highly resolved marsh areas (e.g., 1-meter cross-shore, 5-10 meters along-shore for fringe marshes). The application of unstructured grids to coastal processes offers a great advantage. The superior boundary fitting and local refinement ability of unstructured grids make them ideally suitable for nearshore applications involving complex bathymetry, shoreline geometry, and upland slopes. Figure 3 shows the domain of the unstructured grid used for the model simulations. In addition, TMM has the capacity for a much more dynamic simulation (i.e. rates vary in space and time as determined by changes in the hydrodynamic conditions of the system). Finally, the model highly resolves marsh migration due to the incorporation of anthropogenic stressors, such as coastal development and shoreline armoring.

2.3 Incorporation of a New Vegetation Algorithm in the Tidal Marsh Model

The original version of the TMM (hereafter TMM_**RF**) used a bottom **R**oughness **F**actor (RF) as an indicator of marsh presence (Nunez et al. 2020). Marsh areas were assigned with a RF of 50 mm, while no-marsh areas were designated with a value of 1 mm (Ye et al. 2013).

To increase the functionality of the TMM_RF, we incorporated a vegetation algorithm (Appendix A) in the model to evaluate the effects of *Spartina alterniflora* (dominant plant species in the study areas) on currents and turbulence by modifying the barotropic core of the model. This algorithm allows a more accurate simulation of water flow and turbulence within the marsh. The algorithm was included in the model as an optional function in the simulations. When the vegetation algorithm is turned on, the bottom RF used to define marsh presence is uniformly assigned (1 mm). This is because this factor is less important when compared to form drag from vegetation; with the latter being calculated dynamically inside the model.

Vegetation is modeled as an internal source of resistant force and turbulence energy (Lopez and Garcia 2001; Su and Li 2002). The model uses a semi-implicit time stepping method, and the effect of vegetation is incorporated *implicitly* to maintain model stability at large time steps. Therefore, the stability is independent of the vegetation parameters, and large shears that can develop around the canopy can be efficiently simulated. In addition to the impact of vegetation on flow structure, marsh plants attenuate waves (Mendez and Losada 2004). Wave attenuation by vegetation is taken into account in the wave model inside SCHISM (Zhang et al. 2019).

The inundation frequency used by the TMM_VEG is based on the water-surface level predicted by the modeling system to drive inundation and horizontal marsh migration. Relative SLR is explicitly accounted for in all components. The SLR rate is imposed via the boundary condition at the ocean boundary. The calculated elevation and velocity are shared by all components of the model. The code of the model establishes that marshes have the capability to transgress into an area if the sediment bed elevation is within the suitable elevation range, which is from MSL to 1 m above MSL in our study areas. The CSTMS is responsible to dynamically calculate at each time step the sediment bed elevation, simulating sediment deposition, erosion, and transport. Appendices A, B, and C describe the physical and numerical formulations for the TMM_VEG and the supporting models.

To be consistent with the TMM_RF simulations and evaluation (Nunez et al. 2020), the TMM_VEG was also validated via hindcasting (past 40 years) using a time step of 75 seconds, and the sediment transport model was run with morphological acceleration (i.e., simulation = 1 year; morphological acceleration factor (MAF) = 40). Historic (Moore and Silberhorn 1976; Moore and Silberhorn 1980) and current (CCRM 2018) tidal marsh inventories were employed for the hindcast. The average SLR rate employed for the study areas over the simulation period. for the hindcast was 4 mm yr^{-1} (NOAA Tides and Currents 2018).

2.4 Model Inputs and Outputs

A suite of major inputs needed for the TMM_VEG and supporting models is displayed Table 1. The Tidal Marsh Inventory developed by the Center for Coastal Resources Management (CCRM), Virginia Institute of Marine Science (VIMS) was used to define the current marsh condition for the simulations. The Inventory for the York River is based on a survey conducted in 2010. Marshes were digitized (1:1000 scale) using high resolution, geo-referenced natural color imagery collected in 2009 by the Virginia Base Mapping Program. Marsh boundaries were field checked. This high-resolution dataset was a crucial input in the model to define accurate marsh boundaries.

Table 1. Primary input datasets used for the TMM_VEG and supporting models.

Dataset	**Source**
Historic Tidal Marshes (1:24,000)	Tidal Marsh Inventories – CCRM, VIMS
Current Tidal Marshes (Scale: 1:1,000)	
Shoreline Structures (Scale: 1:1,000)	Shoreline Inventory – CCRM, VIMS
Riparian Land use (distance: 100 ft.)	Shoreline Inventory Program – CCRM, VIMS
LIDAR data	United States Geological Survey (USGS)
Bathymetry	NOAA and CBNERR, VIMS
Bottom Type (grain sizes)	VIMS, Maryland Geological Survey (MGS), and this study - field samples
River Input (average daily values)	United States Geological Survey (USGS)
Total Suspended Solids (average monthly values)	Chesapeake Bay Program
Atmospheric Forcing	North American Regional Reanalysis (NARR)
Tides	US East Coast Tidal Database
Marsh Plant Data	Field Data – CCRM, VIMS

The physical characteristics of marsh plants change seasonally and spatially. In order to reduce model complexity, an average of these characteristics was selected to represent the annual cycle. Average annual values were used because after the plant dies, the stem of *Spartina alterniflora* remains in place and acts as a physical barrier, interfering with the water flow and the sedimentation process until it decomposes.

To determine the dominant marsh plant species in the study areas, the Tidal Marsh Inventory was used to examine the spatial extent and distribution of marsh plant species (CCRM 2018). Spatial analyses were performed in ESRI® ArcGIS 10.6.1 and ArcGIS Pro. Simulations were run using plant data of the dominant plant species in the study areas. *S. alterniflora* physical characteristic, mean values of density, height, and stem diameter were selected to represent the annual cycle, and were input in the vegetation algorithm within the TMM. Marsh plant data (i.e., stem diameter (mm), plant height (cm), and stem density (stem per m^2) were collected to input in the vegetation algorithm (Table 2). Random sampling with quadrats (0.25 m^{-2}) was used to measure stem diameter in the study areas within the low marsh section (*Spartina alterniflora* dominated), for a total of 320 counts. Stem diameter was measured with an electronic digital caliper. Marsh plant height and density data were acquired from surveys in the study areas, as well as other *S. alterniflora*-dominated marshes within the York River watershed to acquire an appropriate representation of the *S. alterniflora* characteristics in this river system. Plant surveys consisted of establishing six transects perpendicular to the seaward edge of the marsh at 13 marshes. Four quadrats (0.25 m^{-2}) were placed along each transect at 1-m intervals from the marsh–estuary edge. Within each quadrat, *S. alterniflora* plant stems were visually counted and the mean height of *S. alterniflora* was recorded for each quadrat sampled (Bilkovic et al. 2017). For this initial version of the TMM_VEG, we assume constant values of plant characteristics. Values of plant height, density, and stem diameter were averaged (i.e., a single value per plant feature) and input in the model.

Table 2 Plant characteristics of *Spartina alterniflora* used as inputs in the TMM_VEG simulations.

Plant Characteristics	Average	Standard Deviation	Count
Density (stem m^{-2})	152	25.5	39 (quadrats)
Height (cm)	76.8	36.0	162 (stems)
Stem diameter (mm)	7.93	2.14	320 (stems)

A great number of outputs are generated by the model, including marsh boundary evolution, distribution of surface marsh sediments, and changes in elevation of the marsh platform. Ancillary outputs from the hydrodynamic, sediment, and wind wave modules include surface and bottom elevations, bed fraction, and wave height, among many others.

2.5 Evaluation of the Enhanced TMM (TMM_VEG)

Model performance with the new vegetation algorithm was assessed by conducting a hindcast (past 40 years). Historic tidal marsh inventories (Moore and Silberhorn 1976; Moore and Silberhorn 1980) and current field observations (CCRM 2018) were used for calibration and verification purposes, focusing on the following aspects: marsh boundary evolution, distribution of surface marsh sediments, and changes in elevation of the marsh platform. In addition, results were compared against the TMM_RF outputs to evaluate if there was a significant difference in model predictions when *Spartina alterniflora* data (TMM_VEG) were used as opposed to a bottom roughness factor (TMM_RF) for marsh presence.

Outputs from the TMM_VEG were exported to the GIS (Geographic Information System) environment using Matlab and Fortran scripts. Spatial analyses were conducted using ESRI® ArcGIS v10.6.1, and ArcGIS Pro.

2.5.1 Marsh Boundary Evolution

The code to simulate the evolution of the marsh boundaries incorporates the effects of tides, waves, sediment transport and morphology, sediment sources, riparian land use, and shoreline armoring. To evaluate the marsh boundary model outputs, the historic Tidal Marsh Inventory generated at VIMS in the early 1970s (Moore and Silberhorn 1976, Moore and Silberhorn 1980), was used in the hindcast as the initial marsh conditions for the simulation. The TMM_VEG was run to the present time, and the marsh boundary outputs were then spatially compared with the current Tidal Marsh Inventory (CCRM 2018). In order to statistically quantify the degree to which the TMM_VEG reproduces the observed data, error matrices were created for both study areas. To be consistent with the approach taken by Nunez et al. (2020), these matrices were used to assess the overall accuracy of the model and to calculate the Kappa statistic (formulation in Appendix D), which is a measure of agreement between the model output and the reference data (i.e., the current Tidal Marsh Inventory). Kappa is a robust statistic and is the most commonly reported measure in evaluating model agreement using categorical variables with multiple levels (McHugh 2012, Tang et al. 2015). In each study area, an error matrix was developed by using 100 random sample points within the marshes. These points were used to establish if the current marsh conditions at those locations agree with the conditions predicted by the TMM_VEG. The random points to assess model performance were the same for both types of simulations (i.e., TMM_RF, and TMM_VEG). In that way, model outputs were directly compared. In addition, the spatial extent and distribution of tidal marshes obtained from the TMM_VEG were mapped, and then compared with the spatial extent and distribution of the model output from the TMM_RF.

2.5.2 Spatial Distribution of Sediments – Grain Size

The spatial distribution of sediments across the marshes was evaluated in the TMM_VEG simulations to determine if including marsh plant data would modify the type of surface sediment fractions accumulated in the marshes. Marsh surface sediment core data were used to validate output from model runs with and without the vegetation component. In both study areas, sediment cores (diameter: 3.5 cm; depth 8 cm) were collected from 20 transects running perpendicular from the water's edge to the marsh-upland zone. Along each transect, three locations were sampled: the marsh-water interface, in the middle of the marsh, and the marsh-upland interface, for a total of 60 cores. Samples were analyzed for grain size employing sieves (Folk 1980, Poppe et al. 2003). Removal of organic carbon and carbonates were conducted using loss on ignition, and HCl acidification of the dried samples (Dean 1974; Heiri et al. 2001; Santisteban et al. 2004), respectively. The Wentworth scale was employed to classify grain size into gravel (2-4 mm), sand (0.062-2 mm), and mud (i.e., silt and clay) (< 0.062 mm). These sediment fractions were directly compared with model outputs.

The ability of the TMM_VEG to reproduce the distribution of the observed marsh surface sediment fractions was evaluated by estimating the Willmott (1982) index of agreement (dr), the mean absolute error of measured values (MAE), the RMSE-standard deviation ratio (RSR), and the coefficient of determination (NSE). Appendix E shows the equations for these statistical performance measures.

2.5.3 Variation in Elevation of the Marsh Platform

The model uses the vertical datum NAVD88 to compute all state variables (e.g., land surface elevation). The changes in elevation (deposition/erosion) were calculated with respect to the initial values. In the study areas, marshes occur within a particular tidal envelope (between MSL and 1m above MSL). MSL (represented by the free water surface) and the land surface elevation vary during the course of the simulation. MSL was adjusted at each model time step by the rate of SLR (i.e., MSL is dynamically calculated). Similarly, land surface elevation was adjusted at each time step through simulation of sediment erosion, transport, and deposition processes. Based on the new MSL and land surface elevations, inundation depth (which equals the difference between the two values) was calculated. The inundation depth was used as a criterion to determine marsh habitat suitability. A new marsh was created in a grid cell if the land surface elevation was between MSL and 1 m above MSL, and at least one adjacent cell was marsh. A marsh grid cell was considered 'drowned' if the land surface elevation fell below MSL.

Changes in elevation of the marsh platform were computed in each study area. The TMM_VEG calculates the variation in elevation of the marsh platform during the simulation period (i.e., depth change from initial marsh surface elevation). Based on these variations, major processes (i.e., "erosion" (negative variation), "deposition" (positive variation), "no change" (variation = 0)) were defined along marsh transects.

2.6 Forecasting Tidal Marsh Evolution

SLR scenarios selected for the forecasts were based on NOAA projections (Sweet et al. 2017). To incorporate subsidence rates in southeast Virginia; an average subsidence rate of 3.1 mm yr-1 (Eggleston and Pope 2013) was added to the projections. For this study, two SLR scenarios were considered: “intermediate” and “extreme.” The intermediate scenario is based on semi-empirical models using statistical relationships in global observations of sea level and air temperature. The extreme scenario is based on estimated consequences from global warming combined with the maximum possible contribution from ice-sheet loss and glacial melting (worst-case scenario). For coastal planning purposes, the projection of marsh evolution in each scenario was 50 years (2020-2070). The increase in sea level by the end of the simulation was 622 mm in the intermediate scenario, and 1,243 mm in the extreme scenario. These two scenarios bound reasonable expectations and provide a larger difference to examine.

The marsh evolution simulations were run with the vegetation algorithm enabled (TMM_VEG) to more accurately assess the water flow and turbulence within the marsh, as well as to better capture the feedback between presence of marsh plants and sediment processes. Vegetation was modeled as an internal source of resistant force and turbulence energy (Lopez and Garcia 2001; Su and Li 2002). In this study, the effect of vegetation on the nearshore hydrodynamics was defined by the presence of the dominant marsh plant species in the study area, *S. alterniflora.* Outputs from the TMM_VEG were exported to the GIS environment using Matlab and Fortran scripts. Spatial analyses were performed using ESRI® ArcGIS 10.6.1 and ArcGIS Pro.

Using a process-based morphodynamic model to conduct long-term simulations involves intensive computational time. This is because morphological changes occur over a much longer time period than hydrodynamic changes. A morphological acceleration factor (MAF) was used to decrease the computational time. This approach was presented by Lesser et al. (2004) and Roelvink (2006), and it is widely used for coastal morphodynamic modeling. This factor was applied after all hydrodynamic and sediment transport processes had been computed for each time step. For the present study, we employed morphological acceleration (i.e., simulation = 1 year; MAF = 50) using a time step of 75 seconds (based on model calibration).

3. Results

3.1 Evaluation of the Enhanced TMM

3.1.1 Marsh Boundary Evolution

The TMM_VEG simulated marsh boundary evolution with an overall high accuracy within both study areas (Carter and Taskinas Creeks: 83%, 82% accuracy; Kappa statistic of 0.69, 0.68, respectively), which indicates "Substantial Agreement" according to Viera and Garrett (2005). Appendix D shows the error matrices comparing TMM_VEG against field observations for Carter Creek and Taskinas Creek. In addition, matrices developed by Nunez et al. (2020) are displayed to facilitate the comparison of model performances between the two different approaches. When using the vegetation algorithm, error matrices show an improvement in the overall accuracy of the model. The Kappa statistic in each study area fell inside the same category ("substantial agreement") based on Viera and Garrett (2005).

Overall, model results were consistent with field observations. The evolution of marsh boundaries derived from both simulations (i.e., with and without the vegetation component) (Figures 4 and 5) reflected the marsh response expected for the study areas during the past 40 years. Marsh migration into open areas was well captured, as were the negative effect of shoreline structures and development on marsh persistence as sea level rises. Marsh loss was significant in areas with high fetch and wave energy in Carter Creek, and outside the mouth of Taskinas Creek, by the main stem of the York River. Nevertheless, including the vegetation algorithm led to a predicted marsh loss of about half of what was predicted without the vegetation component. In Carter Creek, the TMM_RF simulated a marsh loss of 91,459.0 m^2 (net loss 10.2%), while the TMM_VEG simulated a loss of 43,706.1 m^2 (net loss 1.9%). In Taskinas Creek, the TMM_RF simulated a marsh loss of 49,776.3 m^2 (net loss 7.6%) while the TMM_VEG simulated a marsh loss of 26,709.3 m^2 (net loss 3.5%) (Table 3).

Table 3. Marsh areal extent (m^2) after a 40-year simulation (hindcast) using the TMM_RF and the TMM_VEG in Carter Creek and Taskinas Creek.

Simulations	**Marsh Boundary Categories**		
	Marsh Gain (m^2)	No Change (m^2)	Marsh Loss (m^2)
Carter Creek - TMM_RF	24,685.8	56,9797.4	91,459.0
Carter Creek - TMM_VEG	31,160.8	61,7,550.3	43,706.1
Taskinas Creek - TMM_RF	11,735.9	452,033.9	49,776.3
Taskinas Creek - TMM_VEG	9,307.8	475,100.9	26,709.3

3.1.2 Spatial Distribution of Sediments – Grain size

The TMM_VEG sediment outputs had a strong agreement with field observations for both study areas. Similar to the TMM_RF simulation, outputs derived from the TMM_VEG had a good model performance based on the Willmott Modified Index of Agreement and the MAE. The NSE and RSR statistics fall within the satisfactory agreement category based on Singh et al. (2004), and Moriasi et al. (2007) (Appendices E and F). There was not a significant difference between the two model approaches when considering the spatial distribution of grain size throughout the marsh surface. In the case of this particular model output, adding information about the physical characteristics of the marsh plant (plant density, plant height, and stem diameter) in the simulation did not substantially change the predictions about the type of marsh surface sediment fractions (i.e., proportion of gravel, sand, and mud throughout the marsh platform).

3.1.3 Variation in Elevation of the Marsh Platform

The simulation with the vegetation algorithm had an overall lower variation in elevation of the marsh platform in both study areas. In Carter Creek, sites along the marsh transects identified with eroded marsh platform had higher values in the TMM_RF simulation than the TMM_VEG simulation (Figure 6), indicating that the vegetation algorithm more successfully captured the reduction of turbulence, and the capacity of the plants to trap sediments, stabilizing the marsh platform. Appendix G displays the change in elevation of the marsh platform along the marsh transects in Carter Creek when using the TMM_RF and the TMM_VEG, respectively. In some of the sites, the amount of marsh platform lost predicted by the TMM_RF was double or higher than the amount estimated when using the TMM_VEG (e.g., site number 7, 13, 28). Inclusion of vegetation led to reductions in both predicted areal marsh loss and vertical loss of the marsh platform. TMM_RF uses an increased bottom roughness factor (Ye et al. 2013) to assign marsh presence. This uniform bottom roughness (used as marsh plant proxy) interferes with the water mean flow velocity and turbulence, affecting sediment deposition patterns. However, the incorporation of marsh plant data in the vegetation algorithm allowed to better capture the deposition of sediment by marsh plant, stabilizing the marsh platform and resulting in a lower erosion. The incorporation of the physical characteristics of the marsh plants from the study areas provided a more realistic environment affecting the hydrodynamics and the sediment processes, producing a better agreement with the field observations. Most of this behavior occurs in the low-marsh sites (i.e., near the marsh-water interface). These sites are exposed to more frequent and prolonged inundation, allowing more exposure to sediment particles. Nevertheless, a considerable difference in the elevation of the marsh platform was also found in one high-marsh site (site 18). This site is located about 20 meters from the marsh-water edge. The TMM_RF simulation estimated almost a three times higher loss in elevation of the marsh platform. In this case, the difference in model outputs can be related to the higher capacity of the marsh plants to capture sediments coming from the upland-marsh interface due to erosion and/or runoff. In the sites where the dominant process was defined as "deposition," the magnitude of increase in marsh platform elevation did not exhibit a considerable difference between the two model outputs, except for one location (site 20). This site is situated in the middle of a narrow fringe marsh (approximate 5 m wide). The TMM_RF simulation estimated a deposition of 20.2 mm in the 40-year simulation, whereas the model output using the vegetation algorithm predicted an erosion of 2 mm during the same simulation period. This discrepancy in model outputs can be attributed to what was happening to the edge of the marsh (i.e., site 19; low-marsh site) during each of the simulations. In the site 19, the simulation using the roughness factor yielded an erosion of the marsh platform of 106.9 mm in the 40-years simulation, whereas the TMM_VEG simulation projected a loss of 41.1 mm. The TMM_RF simulation produced a greater amount of erosion; hence, more sediments were locally available. These sediments could have been then redeposited in the "new" marsh edge, or further into the existing marsh due to the inundation that reached higher elevations (Friedrichs and Perry 2001; FitzGerald and Hughes 2019; Wiberg et al. 2020;). As mentioned before, deposition of inorganic sediments by marsh plants plays a critical role in maintaining the marsh platform. Incorporating detailed plant information in the vegetation algorithm provided a higher accuracy in the simulation of sediment movement within the marsh, helping to identify areas where erosion or deposition throughout the marsh platform occurred.

A similar pattern was also observed in Taskinas Creek between both simulations. Taskinas Creek presents different hydrodynamics than Carter Creek due to the meandering channels, which result in a particular sedimentation pattern (asymmetrical channel with the deepest part of the channel on the outside of each bend). Both model approaches predicted mostly the same dominant process on the marsh platform (i.e., erosion, deposition, or no change) along the marsh transects. The main exception to this pattern was site 16, located in the low marsh. The simulation using the TMM_RF produced a deposition of 7.0 mm per year, whereas the simulation with TMM_VEG generated a vertical erosion of 11.5 mm per year (Figure 7). Sediment fluxes are not linear functions, so the difference in sediment distribution near this site could have been very different between the two simulations, affecting the local deposition and erosion of the marsh platform. In addition, site 16 is located close to the concave bank, where the stream erodes the sediments, and deposits these and other sediments downstream on the convex bank. This would be the point bar located to the left of site 16. The particular spatial location of this site, as well as differences in sediment fluxes and water flow are some of the reasons that can explain this unique discrepancy. In the case of the deposition process, the magnitude of sediment deposition during the simulation period was either the same for both simulations or a little higher (e.g., site 10) when using the TMM_VEG (due to the enhanced simulation using the vegetation algorithm). Nonetheless, this pattern was not found in sites 13 and 14. This could be attributed to the heterogeneity of the system (i.e., terrain depressions, very narrow marsh channels), which affects plant marsh growth and soil conditions. This particular difference in marsh plant characteristics was not captured by the model due to the underlying assumptions of using only one type of marsh plant community, and assigning constant plant characteristics along the entire marsh. The values of elevation change along the marsh platform in Taskinas Creek are detailed in Appendix G.

3.2 Forecasting Tidal Marsh Evolution

In both study areas, the marsh boundary evolution output was a function of the rate of SLR and the subsequent topographic changes resulting from marsh platform accretion. In many cases, especially in the extreme SLR scenario, the overwhelming extent of inundation damped the impact of topography and flow resistance, and the new marsh patterns were mostly dependent on the rate of SLR. The forecast maps (Figures 8 and 9) show that some marshes had good opportunities to increase their extent by migrating into natural areas that today are not regularly inundated, but that are expected to become inundated in the future.

In Carter Creek, the intermediate SLR scenario projected a marsh loss of 24.2 %. Nevertheless, several marshes were able to migrate inland (16.9 %) and offset part of this loss; hence, yielding a net marsh loss of 7.3% over the next 50 years. The capacity of marshes to transgress was truncated in some areas due to anthropogenic pressure (development, shoreline structures, and roads). The projected marsh response in the extreme SLR scenario was considerably different. By the end of the simulation period, the initial marsh areal extent was reduced by 89.6%. However, due to the local topography and natural riparian upland, many marshes were able to migrate to higher elevations (29.6%) mainly in areas where forested and scrub shrubs have become inundated, resulting in a net marsh loss of 60.0% (Table 4).

In Taskinas Creek, under the intermediate SLR scenario about a quarter of the marshes will be lost, while the vast majority of marshes are expected to be lost under the extreme SLR scenario. The intermediate SLR scenario predicted a marsh loss of 28.8% from the initial marsh coverage. In few areas, marshes were able to transgress (5.7%). This resulted in a net marsh loss of 23.1%. The scenario with the extreme SLR rate projected a major extent of inundation. The initial marsh areal extent decreased by 94.4%. This loss was slightly compensated by some marsh transgression (5.2%), yielding a net loss of 89.2% (Table 4).

Table 4. Projected marsh areal extent (m^2) after a 50-year simulation using an intermediate and extreme scenario of SLR.

	Marsh Boundary Categories		
	Marsh Gain (m^2)	No Change (m^2)	Marsh Loss (m^2)
Carter Creek – Intermediate Scenario	100,766.7	450,819.8	144,068.2
Carter Creek – Extreme Scenario	176,442.9	61,512.2	533,375.8
Taskinas Creek – Intermediate Scenario	27,518.6	342,768.7	138,807.3
Taskinas Creek – Extreme Scenario	25,090.5	26,709.3	454,866.7

4 Discussion

4.1 Evaluation of the Enhanced TMM (TMM_VEG)

We presented a new functionality for a high-resolution and highly predictive marsh evolution model that incorporated physical characteristics of marsh vegetation, topography, sediment dynamics, hydrodynamics, changing sea levels, and human features. The incorporation of a vegetation algorithm into the original version of the TMM (TMM_RF) enhanced the accuracy and predictive capabilities of the model in the majority of the sites evaluated. The effect of marsh plants on the nearshore hydrodynamics provided a different pattern of sediment distribution when compared with the TMM_RF simulations, reflecting an improved agreement between model outputs and field observations. The simulation with marsh plant data better captured sediment deposition and erosion by marsh edges, as shown in the marsh boundary evolution analysis. This type of simulation better reflects the current observed marsh extent and distribution. Moreover, the marsh platforms were more stable due to the effect of marsh plants on sedimentation, as indicated in the elevation change analysis. The type of sediment fractions (i.e., proportion of gravel, sand, mud) throughout the marshes did not differ with the incorporation of the vegetation algorithm, which suggests that the type of inorganic sediments deposited on the marsh platform depends more on the type of sediments available in the system rather than the physical characteristics of the marsh plant, and their capacity to capture sediments.

The enhanced version of the TMM was tested on typical salt marshes dominated by *Spartina alterniflora*. We have demonstrated that using only plant data of the dominant plant species explains the majority of the variability in the salt marsh systems studied. The vegetation algorithm can be modified to incorporate other plant species with different physical characteristics to represent marshes with a different dominant plant species or marshes with a variety of plant species (e.g., freshwater marshes). Spatially assessing and mapping these plant communities and incorporating these data as inputs in the simulations would likely increase the accuracy of the model outputs for those systems.

The development of the model within the SCHISM framework allows for unique model capabilities to be naturally incorporated into the simulations (Nunez et al. 2020). In the original version of the TMM, the authors focused on a 2D barotropic model configuration due to large uncertainties that exist in some marsh process inputs. For processes as complex as marsh migration, it is important to start from a simple approach, investigate the relative importance of contributing factors, and gradually build up model complexity. While the polymorphism in SCHISM allows efficient simulation of marshes in hybrid 2D-3D mode (Liu et al. 2018), the current 2D model already incorporates most of the physics. At this stage, we have achieved with the TMM_VEG an enhanced simulation of changes in marsh position over a 40-year period of observation (hindcast) based on physical processes and factors. A 3D (baroclinic) model that includes salinity and temperature together can further improve the model's predictive capability for the fate of certain marsh species under climate change. Although some sensitivity to grid resolution has been carried out, more analyses on this in the larger context of other uncertainties need to be explored further.

The drag coefficient of marsh vegetation increases in a non-linear way with increasing plant density (Nepf, 1999; Meijer 2005), causing attenuation of wave energy and modification of turbulence. The form drag is dependent on the Reynolds number and on the shape, rigidity and orientation of the object. The TMM_VEG simulations assume a constant value for the drag coefficient. The model code could be modified by adding a varying drag coefficient in the vertical column, which accounts for flexible stems. In the absence of site-specific vegetation data, model results show that implementing a constant value for the drag coefficient is a reasonable approach to evaluate marsh evolution at large scales.

The main limitation of the current version of the model is the application of the model in areas where the current marsh vertical accretion is dominated by organic deposition. Different plant communities have different photosynthetic and decomposition rates, which can directly affect the plant structure and size as well as the root size and distribution. These characteristics will directly affect the capture of sediments and stabilization of the marsh platform by the roots. Due to the variability of marsh plant communities, primary production, and decomposition rates, along with the lack of widespread spatially explicit biological data, we assume biological processes to be constant. While the current version of TMM_VEG does not include biological processes at the moment in the simulations, when considering scenarios with high rates of SLR and long-term projections, the accelerated rates of SLR will surpass the maximum rates of organic deposition by marsh plants, and the fate of marshes will depend only on the availability of inorganic sediments. The focus of this work was to improve the original TMM performance by incorporating the effect of marsh plants on the nearshore hydrodynamics, leaving the assessment of the biological processes for our next stage of model development.

4.2. Forecasting Tidal Marsh Evolution

This study represents an enhanced modeling approach that integrates anthropogenic barriers to marsh migration within a highly-resolved marsh evolution model to simulate realistic marsh sustainability outcomes. The primary drivers of marsh change in different geomorphic and human settings were elucidated from our modeled systems. The application of the TMM with the vegetation algorithm allowed us to develop detailed projections of marsh sustainability in multiple geomorphic settings under different rates of SLR. Across the scenarios evaluated, projections of marsh areal extent vary in both study areas. Major differences in marsh response are mainly attributed to the geomorphic settings, sediment supply, and anthropogenic factors associated with marsh habitats in those tidal systems.

Tidal marshes in Carter Creek occur in a higher topography compared to the ones in Taskinas Creek (Danielson and Tyler 2016). Marshes located at a high topography have more time to offset changes in water levels due to SLR through vertical accretion and horizontal migration, which make them more resilient to SLR (Alizad et al. 2018; Fagherazzi et al. 2019).

The persistence of marsh habitat in Carter Creek in the intermediate scenario can be attributed to the local topography and the sufficient sediment supply in this region, as well as the capacity of the marsh plants to successfully capture and deposit the available sediments onto the marsh platform, increasing its elevation and offsetting the rate of SLR. In the extreme scenario, the accelerated rate of SLR surpassed the rate of vertical accretion by marsh plants in most of the marshes, leading to marsh loss where landward migration was not possible.

In Taskinas Creek, projections of marsh response over the next 50 years were significantly different between the intermediate and extreme scenarios. This can be attributed mainly to the geomorphic setting of this area. Topographic limitations to marsh expansion were more important for this system. Currently, marshes are not only present in a very low elevation, but also are associated with high upland bank height (more than 1.5 m in the majority of the places) and steep slopes, which create an obstacle to inland migration with high rates of SLR. Even though the adjacent upland areas of these marshes are natural, and no anthropogenic stressors are present in this site, the elevated rates of SLR and the physical environment did not allow marshes to migrate horizontally in the majority of places. The estimated area of marsh transgression was almost the same in both forecast scenarios. This suggests that marsh inland migration was mainly truncated by upland bank conditions under accelerated SLR rates. In the extreme SLR scenario, a widespread marsh drowning was observed because migration was limited. The projected sediment supply for this area over the course of the simulation period was not sufficient to increase marsh elevation and to keep pace with SLR.

These projections do not take into account changes in land use and shoreline erosion control structures over the next 50 years, which could significantly change the response of tidal marshes with respect to migrating inland as sea level increases. The conflict between marsh inland migration and human activities near the shoreline is likely to become more significant in the future. Coastal zones are densely populated with an increasing trend of development (Small and Nicholls 2003; Neumannet al. 2015), which will directly affect marsh migration pathways. Shoreline erosion control structures located on the landward edge of the marsh not only act as obstacles for marsh transgression, but also represent barriers for sediment exchange between the marsh and the adjacent upland. Sediment supply is a major factor in marsh response to SLR (Van Proosdij et al. 2006; Cahoon and Guntenspergen 2010; Kolker et al. 2010; Mariotti and Fagherazzi 2010) and a key parameter in modeling marsh evolution (Temmerman et al. 2003b; D'Alpaos et al. 2007a; Kirwan et al. 2016), Lateral and vertical marsh changes can be very sensitive to suspended sediment concentrations. In some settings, small differences in sediment supply can lead to marsh accretion, erosion, progradation, or retreat (Mariotti and Carr 2014; Fagherazzi et al. 2012; Kirwan et al. 2010). The ability of marsh plants to trap sediments increases their resiliency to SLR by maintaining an appropriate surface elevation. Nevertheless, the presence of shoreline armoring to protect private properties from erosion as well as damming of rivers have resulted in a decreased suspended sediment concentration in coastal waters (Willis and Griggs 2003; Weston 2014; Currin et al. 2015). High resolution data sets containing the spatial location of shoreline structures should be included as a model input in the TMM_VEG in order to more accurately simulate sediment deposition by marsh plants and marsh transgression. The code of the TMM_VEG has the capacity to be modified in order to incorporate changes in projections of anthropogenic stressors. If these data are available, we recommend including this information in the forecast to more accurately estimate the future location of marsh habitat.

The projections obtained in our study sites provide a framework of how other marshes might respond under similar geomorphic settings and human activity. This TMM_VEG is exportable; end users are able to easily access the model and tutorials. It can be used in any marsh system to better predict marsh responses under different sea-level rise scenarios, including estuaries, back-barrier islands, fluvially-dominated deltas, and lagoons. For instance, TMM_VEG has the capacity to model horizontal migration that occurs in marshes behind barrier islands. These systems respond to SLR by migrating toward the mainland when sand is overwashed from the barrier island and rolls over onto the back-barrier marsh. The overwash deposition allows marshes to increase in elevation and migrate (Finkelstein and Ferland 1987; Fitzgerald et al. 2007; Walters et al. 2014). However, at rapid and high rates of SLR, barrier island migration can outpace marsh migration toward the mainland, yielding a significant marsh loss (Deaton et al. 2017). The interactions between back barrier marshes and barrier islands play a significant role in determining how coastal systems will evolve in the future due to SLR. Application of the TMM_VEG to this type of systems as well as other regions, and with different marsh plant species, will be mainly limited by the available input data for the target areas. The refinement of the original version of the TMM to simulate marsh evolution will offer coastal managers and other stakeholders a detailed assessment of the fate of tidal marshes in different settings as sea level rises.

The findings produced with the TMM_VEG have other management implications for the Chesapeake Bay region and beyond. Maintaining water quality is one vital service that marshes provide. It is well established that tidal marshes affect water quality by taking up nutrients and trapping sediments (Fisher and Acreman 2004; Mitsch and Gosselink 2007). Excessive loadings of nitrogen, phosphorus, and sediment are of major concern and the focus of the Chesapeake Bay Program, which established total maximum daily loads (TMDLs) (U.S. EPA 2010). To that end, protecting and creating marshes has become especially important for managers trying to achieve water quality goals. Effectiveness in these efforts requires an understanding of how local conditions influence marshes, in particular how the temporal and spatial variation in sediment supply, deposition, and surface erosion can affect the sustainability of these habitats. Because these factors are quite variable in many coastal and estuarine systems, application of a dynamic simulation of marsh evolution with a fine spatial resolution, such as the TMM_VEG, is important for informed management of current and future marsh resources. Furthermore, sedimentation and turbidity are two of the main factors responsible for the decline in populations of North American aquatic organisms (Henley et al. 2010). The capacity of marshes to retain sediments is directly related to their spatial extent and distribution. Understanding how SLR will impact marsh habitats and modify sediment inputs in the system is crucial to maintain and improve water quality and healthy aquatic food webs.

There is an increasing trend from coastal managers and planners to assess the cost-benefit of applying different management strategies to protect marsh habitats and the services that they provide (Kassakian et al. 2017; Reguero et al. 2018; Propato et al. 2018; Rezaie et al. 2020). Another important TMM_VEG application is the identification of areas for marsh conservation that contribute to coastal resilience over longer time frames (e.g., protecting a marsh to reduce coastal erosion, flooding, and/or storm surge impacts). TMM_VEG predictions can be combined with ecosystem-valuation assessments to estimate the most cost-effective strategy to support the physical and ecological services that these critical habitats offer. Model outputs can be used to determine areas at high risk to marsh habitat conversion, as well as potential opportunities for marsh preservation and restoration where upland conditions currently allow transgression. Preserving lands that allow marsh transgression should be a high conservation priority. Coastal managers and decision-makers can use these model outputs to improve the long-term effectiveness of conservation and restoration strategies by maximizing the amount of marsh habitat in high-sediment regions, prioritizing sediment allocation, and identifying and prioritizing key upland transitional sites.

5 Conclusion

A new vegetation component was successfully developed, tested, and incorporated into the Tidal Marsh Model (TMM) to provide an improved simulation of how marsh plants modify the circulation pattern by being an obstacle to water motion, affecting the mean flow velocity and turbulence, and consequently, sedimentation processes. The application of the TMM with the vegetation algorithm advances the spatial modeling and understanding of dynamic SLR effects on tidal marsh vulnerability. Running the TMM with the vegetation algorithm (TMM_VEG) more effectively captures the lateral and vertical changes of tidal marshes, supporting more accurate assessments of the vulnerability of these important resources under present and future conditions. The new version of the TMM is exportable; it can be used in any marsh system to better predict marsh responses under different SLR scenarios. The model code and technical documentation are publicly available via direct download from the SCHISM website: http://ccrm.vims.edu/schismweb/.

Managing shoreline systems to sustain the capacity of marshes to provide multiple ecosystem services entails an understanding of the conditions that will affect their survival. Accelerated rates of SLR will stress the ability of marshes to compensate for rising water levels, and marsh drowning may become more widespread. To better understand the effects of SLR and human pressure on marsh evolution, we projected the changes in marsh extent over the next 50 years in two representative marsh systems within the Chesapeake Bay using the TMM_VEG to incorporate in the simulations the effects of marsh vegetation on the nearshore hydrodynamic. Model outputs show how different coastal settings, such as nearshore topography, sediment supplies, and anthropogenic factors determine the evolution of tidal marshes as the rates of sea level accelerate.

This modeling approach can be used to inform forward-looking management efforts to identify and protect areas where marsh habitats are most likely to be sustainable, as well as preserve opportunities for migration of marsh habitats in an evolving system. These projections provide valuable and necessary information for restoration, strategic planning, and monitoring activities to support marsh sustainability.

Acknowledgement

The authors would like to especially thank William Reay, Eduardo Miles, Kory Angstadt, and Dave Stanhope for their support with field-work activities. We would also like to thank the anonymous reviewers whose comments helped improve the manuscript. This paper has a Contribution No. 1039 of the Virginia Institute of Marine Science, William & Mary.

Funding: This study was supported by the National Oceanic and Atmospheric Administration (grant number NA17NOS4730142), the United States Environmental Protection Agency (grant number CD-96347001-0), the Chesapeake Bay National Estuarine Research Reserve's Rouse-Bottom Fellowship, and the National Science Foundation (grant number 1600131). Any opinions, findings, and conclusions or recommendations expressed in this material are those of the authors and do not necessarily reflect the views of the National Science Foundation.

Some simulations used in this paper were conducted using the following computational facilities: (1) Sciclone at the College of William and Mary which were provided with assistance from the

National Science Foundation, the Virginia Port Authority, Virginia's Commonwealth Technology Research Fund, and the Office of Naval Research; (2) the Extreme Science and Engineering Discovery Environment (XSEDE; Grant TG-OCE130032), which is supported by National Science Foundation grant number OCI-1053575; (3) the NASA High-End Computing (HEC) Program through the NASA Advanced Supercomputing (NAS) Division at Ames Research Center.

Conflicts of interest/Competing interests: The authors declare that they have no conflict of interest.

Code availability: model code can be accessed at http://ccrm.vims.edu/schismweb/

References

Alizad, K., Hagen, S.C., Medeiros, S.C., Bilskie, M.V., Morris, J.T., Balthis, L., et al., 2018. Dynamic responses and implications to coastal wetlands and the surrounding regions under sea level rise. PLoS ONE. 13(10). https://doi.org/10.1371/journal.pone.0205176.

Alizad, K., Hagen, S.C., Morris, J.T, Bacopoulos, P., Bilskie, M.V., Weishampel, J.F., Medeiros, S.C., 2016. A coupled, two-dimensional hydrodynamic-marsh model with biological feedback. Ecol. Modell. 327, 29–43. https://doi.org/10.1016/j.ecolmodel.2016.01.013.

Allen, J,R,L., 2000. Morphodynamics of Holocene salt marshes: A review sketch from the Atlantic and southern North Sea coasts of Europe. Quat. Sci. Rev. 19(12), 1155–1231. https://doi.org/10.1016/S0277-3791(99)00034-7.

Anderson, M.E., Smith, J.M., 2014. Wave attenuation by flexible, idealized salt marsh vegetation. Coastal Engineering. 83, 82–92. https://doi:10.1016/j.coastaleng.2013.10.004.

Barbier, E.B., Hacker, D.H., Kennedy, C., Koch, E.W., Stier, A.C., Silliman, B.R., 2011. The value of estuarine and coastal ecosystem services. Ecol. Monogr. 81, 169–193.

Bennett, N., Croke, B.F.W., Guariso, G., Guillaume, J.H.A., Hamilton, S.H., Jakeman, A.J., Marsili-Libelli, S., Newham, L.T.H., Norton, J.P., Perrin, C., Pierce, S.A., Robson, B., Seppelt, R., Voinov, A.A., Fath, B.D., Andreassian, V., 2013. Characterising performance of environmental models. Environmental Modelling & Software. 40, 1–20. https://doi.org/10.1016/j.envsoft.2012.09.011.

Bilkovic, D.M., Mitchell, M.M., Isdell, R.E., Schliep, M., Smyth, A.R., 2017. Mutualism between ribbed mussels and cordgrass enhances salt marsh nitrogen removal. Ecosphere. 8(4), p.e01795.

Boon, J.D., Mitchell, M., 2015. Nonlinear change in sea level observed at North American tide stations. Journal of Coastal Research. 31(6), 1295–1305. https://doi.org/10.2112/JCOASTRES-D-15- 00041.1

Cahoon, D.R., Guntenspergen, G.R., 2010. Climate change, sea-level rise, and coastal wetlands. National 836 Wetlands Newsletter. 32, 8-12.

Cazenave, A., Nerem, R.S., 2004. Present-day sea level change: Observations and causes. Review of Geophysics. 42, RG3001. https://doi.org/10.1029/2003RG000139.

CCRM (Center for Coastal Resources Management)., 2018. Shoreline & Tidal Marsh Inventory. College of William and Mary. Virginia Institute of Marine Science, Gloucester Point, Virginia. http://www.vims.edu/ccrm/research/inventory/index.php (accessed 15 November 2019).

Clough, J.S., Park, R.A., Fuller, R., 2010. SLAMM 6 beta technical documentation. Warren Pinnacle. http://warrenpinnacle.com/prof/SLAMM6/SLAMM6_Technical_Documentation.pdf (accessed 19 September 2018).

Costanza, R., Pe´rez-Maqueo, O., Martinez, M.L., Sutton, P., Anderson, S.J., Mulder, K., 2008. The value of coastal wetlands for hurricane protection. Ambio. 37, 241–248.

Currin, C., Davis, J., Baron, L.C., Malhotra, A., Fonseca, M., 2015. Shoreline change in the New River Estuary, North Carolina: rates and consequences. J. Coast. Res. 31, 1069–1077. https://doi:10.2112/JCOASTRES-D-14-00127.1.

D'Alpaos, A., Lanzoni, S., Marani, M., Rinaldo, A., 2007a. Landscape evolution in tidal embayments: Modeling the interplay of erosion, sedimentation, and vegetation dynamics. Journal of Geophysical Research. 112. https://doi:10.1029/2006JF000537.

Danielson, J., Tyler, D., 2016. Topobathymetric Model for Chesapeake Bay Region - District of Columbia, States of Delaware, Maryland, Pennsylvania, and Virginia, 1859 to 2015.

Dean, W.E., 1974. Determination of carbonate and organic matter in calcareous sediments and sedimentary rocks by loss on ignition: comparison with other methods. Journal of Sedimentary Petrology. 44, 242-248.

Deaton, C.D., Hein, C.J., Kirwan, M.L., 2017. Barrier-island migration dominates ecogeomorphic feedbacks and drives salt marsh loss along the Virginia Atlantic Coast, USA. Geology. 45, 123–126.

De Jager, J.M., 1994. Accuracy of vegetation evaporation ratio formulae for estimating final wheat 869 yield. Water SA 20(4):307-314. https://hdl.handle.net/10520/AJA03784738_2194 (accessed 5 870 February 2019).

Eggleston, J., Pope, J., 2013. Land subsidence and relative sea level rise in the southern Chesapeake Bay region. US Geological Survey Circular 1392. https://dx.doi.org/10.3133/cir1392.

Enwright, N., Griffith, K/, Osland, M.J., 2016. Barriers to and opportunities for landward migration of coastal wetlands with sea-level rise. Frontiers in Ecology and the Environment 14: 307-316. https://doi.org/10.1002/fee.1282.

Fagherazzi, S., Anisfeld, S.C., Blum, L.K., Long, E.V., Feagin, R.A., Fernandes, A., Kearney, W.S., Williams, K., 2019. Sea level rise and the dynamics of the marsh-upland boundary. Front. Environ. Sci. 7:25. https://doi.org/10.3389/fenvs.2019.00025.

Fagherazzi, S., Kirwan, M.L., Mudd, S.M., Guntenspergen, G.R., Temmerman, S., D'Alpaos, A., van de Koppel, J., et al., 2012. Numerical models of salt marsh evolution: Ecological, geomorphic, and climatic factors. Reviews of Geophysics. 50, RG1002.

Fagherazzi, S., Sun, T., 2004. A stochastic model for the formation of channel networks in tidal marshes. Geophysical Research. Letters. 31, L21503. https://doi.org/10.1029/2004GL020965

Feagin, R.A., Lozada-Bernard, S.M., Ravens, T.M., et al., 2009. Does vegetation prevent wave erosion of salt marsh edges? Proc. Natl. Acad. Sci. U.S.A. 106, 10109–10113.

Finkelstein, K., Ferland, M.A., 1987. Back-barreir response to sea-level rise, eastern shore of Virginia, in: Nummedal, D., Pilkey, O.H., Howard, J.D. (Eds.), Sea-level fluctuation and coastal evolution. SEPM. 41, 145–156.

Fisher, J., Acreman, M.C., 2004. Wetland nutrient removal: a review of the evidence. Hydrology and Earth System Sciences 8:673-685. https://doi.org/10.5194/hess-8-673-2004

FitzGerald, D.M., Zoe H., 2019. Marsh processes and their response to climate change and sea-level rise. Annual Review of Earth and Planetary Sciences. 47(1), 481-517.

FitzGerald, D.M., Howes, N., Kulp, M., Hughes, Z., Georgiou, I., Penland, S., 2007. Impacts of rising sea level to backbarrier wetlands, tidal inlets, and barriers: Barataria Coast, Louisiana. Proceedings of Coastal Sediments 2007 CD-ROM13. pp. 1179-1192.

Folk, R.L., 1980. Petrology of sedimentary rocks. Hemphill Publishing Company, Austin, TX.

Friedrichs, C.T., Perry, J.E.,2001. Tidal salt marsh morphodynamics: a synthesis. Journal of Coastal Research. 7-37.

Gedan, K.B., Kirwan, M.L., Wolanski, E., Barbier, E.B., Silliman, B.R., 2011. The present and future role of coastal wetland vegetation in protecting shorelines: answering recent challenges to the paradigm. Clim. Change. 106, 7–29.

Gittman, R.K., Fodrie, J., Popowich, A.M., Keller, D.A., Bruno, J.F., Currin, C.A., Peterson, C.H., Piehler, M.F., 2015. Engineering away our natural defenses: An analysis of shoreline hardening in the US. Frontiers in Ecology and the Environment 13(6):301 307. https://dx.doi.org/10.1093%2Fbiosci%2Fbiw091.

Hall, J.A., Gill, S., Obeysekera, J., Sweet, W., Knuuti, K., Marburger, J., 2016. Regional sea level scenarios for coastal risk management: managing the uncertainty of future sea level change and extreme water levels for Department of Defense Coastal Sites Worldwide. U.S. Department of Defense, Strategic Environmental Research and Development Program.

Heiri, O., Lotter A.F., Lemcke, G., 2001. Loss on ignition as a method for estimating organic and carbonate content in sediments: reproducibility and comparability of results. Journal of Paleolimnology. 25, 101-110.

Henley, W.F., Patterson, M.A., Neves, R.J., Lemly, A.D., 2010. Effects of Sedimentation and Turbidity on Lotic Food Webs: A Concise Review for Natural Resource Managers. Journal Reviews in Fisheries Science 8: 125-139. https://doi.org/10.1080/10641260091129198.

Hill, K., 2015. Coastal infrastructure: a typology for the next century of adaptation to sea-level rise. Frontiers in Ecology and the Environment 13 (9):468-476. https://doi.org/10.2112/07A-0010.1.

Horton, B., Shennan, I., Bradley, S.L., Cahill, N., Kirwan, M., Kopp, R.E., Shaw, T.A., 2018. Predicting marsh vulnerability to sea-level rise using Holocene relative sea-level data. Nature Communications. 9(1), 2697-2690. https://doi.org/10.1038/s41467-018-05080-0.

John, B.M., Shirlal, K.G., Rao, S., 2015. Effect of artificial vegetation on wave attenuation – an experimental investigation. Procedia Eng. 116, 600–606. https://doi:10.1016/j.proeng.2015.08.331.

Kassakian, J., Jones, A., Martinich, J. et al., 2017. Managing for no net loss of ecological services: an approach for quantifying loss of coastal wetlands due to sea level rise. Environmental Management. 59, 736–751. https://doi.org/10.1007/s00267-016-0813-0.

Kirwan, M., Walters, D.C., Reay, W.G., Carr, J.A., 2016. Sea level driven marsh expansion in a coupled model of marsh erosion and migration. Geophysical Research Letters. 43, 4366–4373. https://doi.org/10.1002/ 2016GL068507.

Kirwan, M.L., Guntenspergen, G.R., D'Alpaos, A., Morris, J.T., Mudd, S.M., Temmerman, S., 2010. Limits on the adaptability of coastal marshes to rising sea level. Geophysical Research Letters. 37, 5. https://doi:201010.1029/2010GL045489.

Kirwan, M.L., Murray, A.B., 2007. A coupled geomorphic and ecological model of tidal marsh evolution. Proceedings of the National Academy of Sciences. 104(15), 6118–6122. https://doi.org/10.1073/pnas.0700958104.

Kiss, M., Jozsa, J., 2014. Measurement-based hydrodynamic characterization of reed – open water interface zones in shallow lake environment. Per. Pol. Civil Eng. 58, 229-241.

Kolker, A.S., Kirwan, M.L., Goodbred, S.L., Cochran, J. K., 2010. Global climate changes recorded in coastal 951 wetland sediments: empirical observation linked to theoretical predictions. Geophys. Res. Lett. 37, 952.

Leonard, L.A., Croft, A.L., 2006. The effect of standing biomass on flow velocity and turbulence in Spartina alterniflora canopies, Estuarine Coastal Shelf Sci. 69(3–4), 325–336.

Leonardi, N., Fagherazzi, S., 2014. How waves shape salt marshes. Geology. https://doi.org/10.1130/G35751.1.

Le Roux, D.Y., 2012. Spurious inertial oscillations in shallow-water models. Journal of Computational 965 Physics. 231, 7959–7987. https://doi.org/10.1016/j.jcp.2012.04.052.

Lesser, G.R., Roelvink, J.A., Van Kester, J., Stelling, G.S., 2004. Development and validation of a three-dimensional morphological model. Coastal Engineering. 51(8-9), 883–915.

Liu, Q., Anderson, E., Zhang, Y.J., Weinke, A.D., Knapp, K.L., Biddanda, B.A., 2018. Modeling reveals the role of coastal upwelling and hydrologic inputs on biologically distinct water exchanges in a Great Lakes estuary. Estuarine, Coastal and Shelf Science. 29, 41-55. https://doi.org/10.1016/j.ecss.2018.05.014.

Lopez, F., Garcia, M., 2001. Mean flow and turbulence structure of open-channel flow through non-emergent vegetation. Journal of Hydraulic Engineering. 127(5), 392 – 402.

Machiwal, D., Jha, M.K., 2015. GIS-based water balance modeling for estimating regional specific yield 979 and distributed recharge in data-scarce hard-rock regions. Journal of Hydro-Environment Research. 980 9(4), 554–568. http://dx.doi.org/10.1016%2Fj.jher.2014.07.004.

Mariotti, G., Fagherazzi, S., Wiberg, P.L., McGlathery, K.J., Carniello, L., Defina, A., 2010. Influence of storm surges and sea level on shallow tidal basin erosive processes. Journal of Geophysical Research. 115 C11012. https://doi.org/10.1029/2009JC005892.

Mariotti, G,, Carr, J., 2014. Dual role of salt marsh retreat: long-term loss and short-term resilience. Water Resources Research. 50, 2963–2974. https://doi.org/10.1002/2013WR014676.

Marsooli, R., Wu, W., 2014. Numerical investigation of wave attenuation by vegetation using a 3D RANS model. Advances in Water Resources. 74, 245–257. https://doi.org/10.1016/j.advwatres.2014.09.012.

McHugh, M., 2012. Interrater reliability: the kappa statistic. Biochemia Medica. 22(3), 276–282. https://doi.org/10.11613/bm.2012.031.

Mcleod, E., Poulter, B., Hinkel, J., Reyes, E., Salm, R., 2010. Sea-level rise impact models and environmental conservation: A review of models and their applications. Ocean and Coastal Management. 53(9), 507–517. https://doi.org/10.1016/j.ocecoaman.2010.06.009.

Meijer, M.C., 2005. Wave attenuation over salt marsh vegetation, Master's thesis, TU Delft.

Mendez, F., Losada, I.J., 2004. An empirical model to estimate the propagation of random breaking and nonbreaking waves over vegetation fields. Coast Eng. 51, 103–118. https://doi.org/10.1016/j.coastaleng. 2003.11.003.

Mitsch, W.J., Gosselink, J.G., 2007. Wetlands. 4th edn. John Wiley & Sons.

Mogensen, L.A., Rogers, K., 2018. Validation and comparison of a model of the effect of sea-level rise on coastal wetlands. Sci Rep. 8, 1369. https://doi.org/10.1038/s41598-018-19695-2.

Moore, K.A., Silberhorn, G.M., 1980. James City County tidal marsh inventory. Special Reports in Applied Marine Science and Ocean Engineering No. 188. Virginia Institute of Marine Science, College of William and Mary. https://doi.org/10.21220/V54H8T.

Moore, K.A., Silberhorn, G.M., 1976. Gloucester County tidal marsh inventory. Special Report in Applied Marine Science and Ocean Engineering No. 64. Virginia Institute of Marine Science, College of William and Mary. https://doi.org/10.21220/V5972B.

Moriasi, D., Arnold, J., Van Liew, M., Bingner, R., Harmel, D., Veith, T., 2007. Model evaluation guidelines 1015 for systematic quantification of accuracy in watershed simulations. Transactions of the American 1016 Society of Agricultural and Biological Engineers. 50(3), 885-900. https://doi.org/ 10.13031/2013.23153.

Morris, J.T., Sundareshwar, P.V., Nietch, C.T., Kjerfve, B., Cahoon, D.R., 2002. Responses of coastal wetlands to rising sea level. Ecology. 83(10), 2869–2877. https://doi.org/ 10.1890/0012-9658(2002)083[2869:ROCWTR]2.0.CO;2.

Nepf, H.M., Vivoni, E.R., 2000. Flow structure in depth-limited, vegetated flow. Journal of Geophysical Research. 105(C12), 28547-28557.

Nepf, H.M., 1999. Drag, turbulence and diffusion in flow through emergent vegetation. Water Resour. Res. 35(2), 479–489. https://doi.org/10.1029/1998WR900069.

Neumann, B., Vafeidis, A., Zimmermann, J., 2015. Future coastal population growth and exposure to sea-level rise and coastal flooding-a global assessment. PLOS ONE. 10(6), e0131375. https://doi.org/10.1371/journal.pone.0131375.

NOAA Tides and Currents., 2018. Relative sea level trend 8638610 Sewells Point, Virginia. https://tidesandcurrents.noaa.gov/sltrends/sltrends_station.shtml?id=8638610 (accessed 11 November 2018).

Nunez, M. K., 2020. Cross-scale simulations: an innovative approach to evaluate the impacts of sea-level rise on tidal marsh habitats. ProQuest Dissertations Publishing. The College of William and Mary, ProQuest Dissertations Publishing, 27955662. http://dx.doi.org/10.25773/v5-e0me-b363.

Nunez, K., Zhang, Y., Herman, J., Reay W, Hershner C., 2020. A Multi-scale Approach for Simulating Tidal Marsh Evolution. Ocean Dynamics, 70(9), 1187–1209. https://doi.org/10.1007/s10236-020-01380-6.

Odink, S.J., 2019. Long-term marsh growth and retreat in an online coupled hydrodynamic, morphodynamic and ecological model. Master Thesis in Water Engineering and Management. Faculty of Engineering Technology. University of Twente. The Netherlands.

Parris, A., Bromirski, P., Burkett, V., Cayan, D., Culver, M., Hall, J., Horton, R., Knuuti, K., Moss, R., Obeysekera, J., Sallenger, A., Weiss, J., 2012. Global sea level rise scenarios for the US National climate assessment. NOAA Tech Memo OAR CPO-1.

Pinto, L., Fortunato, A.B., Zhang, Y., Oliveira, A., Sancho, F.E.P., 2012. Development and validation of a three-dimensional morphodynamic modelling system for non-cohesive sediments. Ocean Model. 57- 58, 1–14. https://doi.org/10.1016/j.ocemod.2012.08.005.

Poppe, L.J., Eliason, A.H., Fredericks, J.J., Rendigs, R.R., Blackwood, D., Polloni, C.F., 2003. Grain-size analysis of marine sediments: methodology and data processing. In Open File Report 00-358, Chapter 1. U.S. Geological Survey. https://pubs.usgs.gov/of/2000/of00-358/text/chapter1.htm (accessed 12 December 2018).

Propato, M., Clough, J. S., Polaczyk, A., 2018. Evaluating the costs and benefits of marsh-management strategies while accounting for uncertain sea-level rise and ecosystem response. PloS one. 13(8), e0200368. https://doi.org/10.1371/journal.pone.0200368.

Raposa, K., Ekberg, M.L.C., Burdick, D., Ernst, N.T., Adamowicz, S.C., 2017. Elevation change and the vulnerability of Rhode Island (USA) salt marshes to sea-level. Regional Environmental Change. 17, 389–397. https://doi.org/10.1007/s10113-016-1020-5.

Rahmstorf, S., 2007. A semi-empirical approach to projecting future sea-level rise. Science. 315(5810), 368–70.

Reed, D.J., 1995. The response of coastal marshes to sea-level rise: survival or submergence? Earth Surface Processes and Landforms. 20, 39–48. https://doi.org/10.1002/esp.3290200105.

Reguero, B.G., Beck, M.W., Bresch, D.N., Calil, J., Meliane, I., 2018. Comparing the cost effectiveness of nature-based and coastal adaptation: A case study from the Gulf Coast of the United States. PLoS One, e0192132. https://doi.org/10.1371/journal.pone.0192132.

Rezaie, A. M., Loerzel, J., Ferreira, C. M., 2020. Valuing natural habitats for enhancing coastal resilience: Wetlands reduce property damage from storm surge and sea level rise. PloS one. 15(1), e0226275. https://doi.org/10.1371/journal.pone.0226275.

Roelvink, D.J.A., 2006. Coastal morphodynamic evolution techniques. Coastal Engineering. 53(2-3), 277–287.

Roland, A., Zhang, Y.J., Wang, H.V., Meng, Y., Teng, Y.C., Maderich, V., Brovchenko, I., Dutour-Sikiric, M., Zanke, U., 2012. A fully coupled 3D wave-current interaction model on unstructured grids. Journal of Geophysical Research. 177, 1-18. https://doi.org/10.1029/2012JC007952.

Roland, A., 2009. Development of WWM II: spectral wave modeling on unstructured meshes. Ph.D. thesis, Technische Universit¨at Darmstadt, Institute of Hraulic and Water Resources Engineering.

Roland, R.M., Douglass, S.L., 2005. Estimating wave tolerance of Spartina alterniflora in coastal Alabama. Journal of Coastal Research. 21(3), 453 – 463.

Santisteban, J.I., Mediavilla, R., López-Pamo, E., Dabrio, C.J., Zapata, M.B.R., García, M.J.G., Castaño, S., Martínez-Alfaro, P.E., 2004. Loss on ignition: a qualitative or quantitative method for organic matter and carbonate mineral content in sediments?. Journal of Paleolimnology. 32, 287-299.

Shepard, C.C., Crain, C.M., Beck, M.W., 2011. The protective role of coastal marshes: a systematic review and meta-analysis. PLoS ONE. 6(11), e27374,1-11. https://doi.org/10.1371/journal.pone.0027374.

Silliman, B.R., Schrack, E., He, Q., Cope, R., Santoni, A., van der Heide, T., Jacobi, R., Jacobi, M., van de Koppel, J., 2015. Facilitation shifts paradigms and can amplify coastal restoration efforts. Proceedings of the National Academy of Sciences of the United States of America. 112, 4295–14300.

Singh, J., Knapp, V., Demissie, M., 2004. Hydrologic modeling of the Iroquois River watershed using 1094 HSPF and SWAT. ISWS Contract Report CR 2004-08. Illinois State Water Survey. http://www.isws.illinois.edu/pubdoc/CR/ISWSCR2004-08.pdf (accessed 22 November 2019).

Spalding, M.D., McIvor, A.L., Beck, M.W., et al., 2014. Coastal ecosystems: a critical element of risk reduction. Conserv. Lett. 7, 293–301.

Small, C., Nicholls, R.J., 2003. A global analysis of human settlement in coastal zones. J. Coast. Res. 19, 584–599.

Su, X.H., Li, C.W., 2002. Large eddy simulation of freee surface turbulent flow in partly vegetated open channels. International Journal for Numerical Methods in Fluids. 39,919-937.

Sutton-Grier, A.E., Wowk, K., Bamford, H., 2015. Future of our coasts: the potential for natural and hybrid infrastructure to enhance the resilience of our coastal communities, economies and ecosystems. Environ. Sci. Policy. 51, 137–148

Sweet, W.V., Kopp, R.E., Weaver, C.P., Obeysekera, J., Horton, R., Thieler, E.R., Zervas, C., 2017. Global and regional sea level rise scenarios for the United States (Tech. Rep. NOS CO-OPS 083). Silver Spring, MD: National Oceanic and Atmospheric Administration.

Tang, W., Hu, J., Zhang, H., Wu, P., He, H., 2015. Kappa coefficient: A popular measure of rater agreement. Shanghai Archives of Psychiatry. 27(1), 62–67.

Temmerman, S., Bouma, T.J., Govers, G., Wang, Z.B., De Vries, M.B., Herman, P.M.J., 2005. Impact of vegetation on flow routing and sedimentation patterns: three-dimensional modeling for a tidal marsh. J. Geophys Res. 110, F04019. https://doi.org/10.1029/2005JF000301.

Temmerman, S., Goers, G., Wartel, S., Meire, P., 2003b. Spatial and temporal factors controlling short term sedimentation in a salt and freshwater tidal marsh, Scheldt Estuary, Belgium, SW Netherlands, Earth Surf. Processes Landforms. 28, 739–755. https://doi.org/10.1002/esp.495.

Titus, J.G., Anderson, K.E., Cahoon, D.R., Gesch, D.B., Gill, S.K., Gutierrez, B.T., Thieler, E.R., William, S.J., 2009. Coastal sensitivity to sea-level rise: a focus on the mid-atlantic region. U.S. Climate Change Science Program and the Subcommittee on Global Change Research. Washington, D.C.

Umlauf, L., Burchard, H., 2003. A generic length-scale equation for geophysical turbulence models. Journal Marine Research. 6, 235-265. https://doi.org/10.1357/002224003322005087.

United States Environmental Protection Agency (U.S. EPA)., 2010. Chesapeake Bay TMDL Document) https://www.epa.gov/chesapeake-bay-tmdl/chesapeake-bay-tmdl-document (accessed 25 January 2019).

Van Proosdij, D., Davidson-Arnott, R.G.D., Ollerhead, J., 2006. Controls on spatial patterns of sediment 1142 deposition across a macro-tidal salt marsh surface over single tidal cycles. Estuarine Coastal Shelf Sci. 1143 69, 64–86. https://doi.org/10.1016/j.ecss.2006.04.022.

Viera, A.J., Garrett, J.M., 2005. Understanding inter observer agreement: the kappa statistic. Family Medicine. 37(5), 360-363.

Walters, D., Moore, L.J., Durán, O., Fagherazzi, S., Mariotti, G., 2014. Interactions between barrier islands and backbarrier marshes affect island system response to sea level rise: Insights from a coupled model. J. Geophys. Res. 119, 2013–2031.

Warner, J.C., Sherwood, C.R., Signell, R.P., Harris, C.K., Arango, H.G., 2008. Development of a three-dimensional, regional, coupled wave, current, and sediment-transport model. Computers & Geosciences. 34, 1284-1306. https://doi.org/10.1016/j.cageo.2008.02.012.

Weston, N.B., 2014. Declining sediments and rising seas: an unfortunate convergence for tidal wetlands. Estuaries Coasts. 37, 1–23.

Wiberg, P.L., Fagherazzi, S., Kirwan, M.L., 2020. Improving predictions of salt marsh evolution through better integration of data and models. Ann Rev Mar Sci. 3(12), 389-413. https://doi.org/10.1146/annurev-marine-010419-010610.

Willis, C.M., Griggs, G.B., 2003. Reductions in fluvial sediment discharge by coastal dams in California and implications for beach sustainability. The Journal of Geology. 111, 167-182.

Willmott, C.J., Robeson, S.M., Matsuura, K., Ficklin, D.L., 2012. Short communication: a refined index of model performance. International Journal of Climatology. 32, 2088-2094. https://doi.org/10.1002/joc.2419.

Willmott, C.J., 1982. Some comments on the evaluation of model performance. Bulletin of the American Meteorological Society. 63, 1309–1313. https://doi.org/10.1175/1520-0477(1982)063%3C1309:SCOTEO%3E2.0.CO;2.

Ye, F., Chen, Q., Blanckaert, K., Ma, J., 2013. Riparian vegetation dynamics: Insight provided by a process-based model, a statistical model and field data. Ecohydrology. 6, 567–85. https://doi.org/10.1002/eco.1348.

Ysebaert, T., Yang, S.L., Zhang, L., He, Q., Bouma, T.J., Herman, P.M.J., 2011. Wave attenuation by two contrasting ecosystem engineering saltmarsh macrophytes in the intertidal pioneer zone. Wetlands. 31, 1043–1054. https://doi.org/10.1007/s13157-011-0240-1.

Zedler, J.B., Kercher, S., 2005. Wetland resources: status, trends, ecosystem services, and restorability Annual Review of Environment and Resources. 30, 39–74. https://doi.org/10.1146/annurev.energy.30.050504.144248.

Zhang, Y., Gerdts, N., Ateljevich, E., Nam, K., 2019. Simulating vegetation effects on flows in 3D using an unstructured grid model: model development and validation. Ocean Dynamics. 70, 213-230. https://doi.org/10.1007/s10236-019-01333-8.

Zhang, Y.J., Ye, F., Staney, E.V., Grashorn, S., 2016. Seamless cross-scale modeling with SCHISM. Ocean Modelling. 102, 64-81. https://doi.org/10.1016/j.ocemod.2016.05.002.

Zhu, Z., Bouma, T.J.; Ysebaert, T., Zhang, L., Herman, P.M.J., 2014. Seed arrival and persistence at the tidal mudflat: identifying key processes for pioneer seedling establishment in salt marshes. Mar. Ecol. Prog. Ser. 513, 97-109https://dx.doi.org/10.3354/meps10920.

APPENDICES

Appendix A - TMM (RF &VEG) Physical Formulation – Governing equations:

SCHISM solves the 3D Reynolds-averaged Navier-Stokes equation in its hydrostatic form:

Momentum equation: $\frac{D\mathbf{u}}{Dt} = \frac{\partial}{\partial z}\left(\nu \frac{\partial \mathbf{u}}{\partial z}\right) - g\nabla\eta + \mathbf{F}$

Continuity equation in 3D and 2D depth-integrated forms: $\nabla \cdot \mathbf{u} + \frac{\partial w}{\partial z} = 0$

$$\frac{\partial \eta}{\partial t} + \nabla \cdot \int_{-h}^{\eta} \mathbf{u}dz = 0$$

Transport equation:

$$\frac{\partial C}{\partial t} + \nabla \cdot (\mathbf{u}C) = \frac{\partial}{\partial z}\left(\kappa \frac{\partial C}{\partial z}\right) + F_h,$$

Equation of state:

$\rho = \rho(S, T, p)$

where

∇	$\left(\frac{\partial}{\partial x}, \frac{\partial}{\partial y}\right)$
D/Dt	material derivative (s^{-1})
(x,y)	horizontal Cartesian coordinates (m)
z	vertical coordinate, positive upward (m)
t	time (s)
$\eta(x,y,t)$	free-surface elevation (m)
$h(x,y)$	bathymetric depth (m)
$\mathbf{u}(x,y,z,t)$	horizontal velocity, with Cartesian components (u,v)
w	vertical velocity
$\boldsymbol{F}$	other forcing terms in momentum (baroclinic gradient $(-\frac{g}{\rho_0}\int_z^{\eta}\nabla\rho d\zeta)$, horizontal viscosity, Coriolis, earth tidal potential, atmospheric pressure, radiation stress)
g	acceleration of gravity, in (ms^{-2})
C	tracer concentration (e.g., salinity, temperature, sediment, etc.)
ν	vertical eddy viscosity, in (m^2s^{-1})
κ	vertical eddy diffusivity, for tracers, in (m^2s^{-1})
F_h	horizontal diffusion and mass sources/sinks

As previously stated, a simpler 2D barotropic configuration was used in this study.

Particular Case – Evaluation of Marsh Pants on Nearshore Hydrodynamics (TMM_VEG)

Based on Zhang et al. (2019) the Reynold's Averaged Navier-Stokes equations are modified by adding a form drag term due to vegetation:

$$\frac{Du}{dt} = f - g\nabla\eta + m_z - \alpha|u|uL\ (x, y, z)$$

$$\alpha(x, y) = Di_v\, N_v C_{DV}/2$$

Where:

u = horizontal velocity

D/dt = material derivative

g = gravitational acceleration

η = surface elevation

α = vegetation related variable

m_z= vertical eddy viscosity term

L = vegetation term

Di_v = stem diameter

N_v = vegetation density (number of stems per m^2)

C_{DV} = bulk form drag coefficient (Nepf and Vivoni, 2000) (value used = 1.13)

f = includes a number of explicitly treated terms (e.g., Coriolis, baroclinic pressure gradient, horizontal viscosity).

Since SCHISM allows 'polymorphism' with mixed 2D and 3D cells in a single grid (Zhang et al. 2016), there are different forms for the vertical eddy viscosity term (m_z).

$$\boldsymbol{m}_z = \begin{cases} \frac{\partial}{\partial z}\left(\nu \frac{\partial \boldsymbol{u}}{\partial z}\right), & 3D\ cells \\ \frac{\boldsymbol{\tau_w} - \chi \boldsymbol{u}}{H}, & 2D\ cells \end{cases}$$

The vegetation term:

$$L(x,y,z) = \begin{cases} \mathcal{H}(z_v - z), & 3D \\ 1, & 2D \end{cases}$$

ν = eddy viscosity

τ_w = the surface wind stress

$H=h+\eta$ is the total water depth (with h being the depth measured from a fixed datum)

$\chi = C_D|\boldsymbol{u}|$, C_D = the bottom drag coefficient

z_v = the z-coordinate of the canopy.

Note that $\boldsymbol{u}$ denotes the depth-averaged velocity in a 2D region.

$\mathcal{H}()$ = the Heaviside step function

$$\mathcal{H}(x) = \begin{cases} 1, x \geq 0 \\ 0, x < 0 \end{cases}$$

Appendix B - TMM Numerical Formulation: Geometry and Discretization

SCHISM-TMM is a finite-element model that uses a flexible unstructured grid (UG). For the horizontal grid, hybrid triangular-quadrangular (quads) elements are employed to take advantage of the superior boundary-fitting capability of triangles as well as efficiency/accuracy of quads in representing certain features (e.g., channels) as needed.

The basic 3D computational unit in SCHISM is a triangular prism or quad prism. Surface elevations (η) are defined at the nodes, and the horizontal velocities (u, v) are defined at the side centers and whole levels. The vertical velocity (w) is defined at the element centers and whole levels, and the tracer concentration (C) is defined at prism center, as it is solved with a finite volume method. The conformal and non-conformal linear shape functions (Le Roux 2012) are used for elevations and velocities respectively.

Boundary Conditions. The differential equations previously described require initial conditions (I.C.) and boundary conditions (B.C.). Generally, all state variables (η,u,C) are specified at t=0 as I.C. In addition, some variables are specified at all open lateral boundary segments (e.g. open ocean, rivers, etc.). At the sea-surface interface, SCHISM enforces the balance between the internal Reynolds stress and the applied shear stress:

$$\nu\, \partial \boldsymbol{u}\, \partial z = \boldsymbol{\tau}_w, \quad z = \eta$$

Since the bottom boundary layer is typically not well resolved in ocean models, the no-slip condition at the sea or river bottom (u = w = 0) is replaced by a balance between the internal Reynolds stress and the bottom frictional stress,

$$\nu\, \partial \boldsymbol{u}\, \partial z = \boldsymbol{\tau}_b,\ at\ z = -h.$$

For a turbulent boundary layer, the bottom stress is defined as:

$$\boldsymbol{\tau}_b = C_D |\boldsymbol{u}_b| \boldsymbol{u}_b$$

where $\boldsymbol{u}_b$ is the near bottom velocity.

Turbulence closure. The momentum equation and transport equation are not closed and must be supplemented by turbulence closure equations for the viscosity/diffusivity. SCHISM uses the Generic Length-Scale (GLS) model of Umlauf and Burchard (2003) with proper I.C. and B.C. for each differential equation.

Appendix C. Main Equations for Supporting Models

Suspended Sediment Transport. Suspended sediment concentrations are computed as follows (Pinto et al. 2012):

$$\frac{\partial c_j}{\partial t} + \nabla_h \cdot (\boldsymbol{u} c_j) + \frac{\partial[(w - w_{sj})c_j]}{\partial z} = \frac{\partial}{\partial z}\left(\kappa \frac{\partial c_j}{\partial z}\right) + F_h$$

c_j - volume concentration of suspended sediment in class j
u - horizontal velocity
$\boldsymbol{\kappa}$ - eddy diffusivity
w_{sj} - settling velocity
$\boldsymbol{F_h}$ - horizontal mixing

Spectral Wave Model (WWM-III). Governing equation for wave action is defined as (Ronald et al. 2012):

$$\underbrace{\frac{\partial}{\partial t} N}_{\text{Change in Time}} + \underbrace{\nabla_x (XN)}_{\text{Advection in horizontal space}} + \underbrace{\frac{\partial}{\partial \sigma}(\theta N) \quad \frac{\partial}{\partial \theta}(\sigma N)}_{\text{Advection in spectral space}} = \underbrace{S_{tot}}_{\text{Total Source Term}}$$

where:

$$N_{(t,X,\sigma,\theta)} = \frac{E_{(t,X,\sigma,\theta)}}{\sigma}$$

E = variance density of the sea level elevations
σ = relative wave frequency
θ = wave direction
X = Cartesian coordinate vector (x, y) in the geographical space

Appendix D. Error matrices (TMM_REF and TMM_VEG)

Table D.1 Error matrices for Carter Creek based on 100 random sample points. The upper matrix displays the model results using the vegetation algorithm (**TMM_VEG**); the lower matrix display model outputs using a roughness factor (**TMM_RF**). Each point was used to evaluate if the current marsh conditions at that location agree with the conditions predicted by the model. Bold numbers in the diagonal represents the counts where model outputs and current conditions agree.

CARTER CREEK		CURRENT TIDAL MARSH INVENTORY				
		No Change	Marsh Gain	Marsh Loss	TOTAL	Commission Error
	No Change	**52**	2	9	63	0.17
TIDAL MARSH MODEL	Marsh Gain	1	**9**	0	10	0.10
(TMM_VEG)	Marsh Loss	5	0	**22**	27	0.19
	TOTAL	58	11	31	**100**	
	Omission Error	0.10	0.18	0.29		**0.17**

CARTER CREEK		CURRENT TIDAL MARSH INVENTORY				
		No Change	Marsh Gain	Marsh Loss	TOTAL	Commission Error
	No Change	**45**	2	7	54	0.17
TIDAL MARSH MODEL	Marsh Gain	2	**8**	0	10	0.20
(**TMM_RF**)	Marsh Loss	8	0	**28**	36	0.22
	TOTAL	**55**	**10**	**35**	**100**	
	Omission Error	0.18	0.20	0.20		**0.19**

Table D.2 Error matrices for Taskinas Creek based on 100 random sample points. The upper matrix displays the model results using the vegetation algorithm (**TMM_VEG)**; the lower matrix display model outputs using a roughness factor (**TMM_RF**). Each point was used to evaluate if the current marsh conditions at that location agree with the conditions predicted by the model. Bold numbers in the diagonal represents the counts where model outputs and current conditions agree.

TASKINAS CREEK		CURRENT TIDAL MARSH INVENTORY				
		No Change	Marsh Gain	Marsh Loss	TOTAL	Comission Errror
TIDAL MARSH MODEL (**TMM_VEG**)	No Change	**50**	5	7	62	0.19
	Marsh Gain	1	**19**	0	20	0.05
	Marsh Loss	5	0	**13**	18	0.28
	TOTAL	56	24	20	**100**	
	Omission Error	0.11	0.79	0.35		**0.18**

TASKINAS CREEK		CURRENT TIDAL MARSH INVENTORY				
		No Change	Marsh Gain	Marsh Loss	TOTAL	Commission Error
TIDAL MARSH MODEL (**TMM_RF**)	No Change	**48**	5	6	59	0.19
	Marsh Gain	3	**16**	0	19	0.16
	Marsh Loss	8	0	**14**	22	0.36
	TOTAL	59	21	20	**100**	
	Omission Error	0.19	0.24	0.30		0.22

Where Kappa statistic (K):

$$K = \frac{N\sum_{i=1}^{k} x_{ii} - \sum_{i-1}^{k}(x_{1+} X\, x_{+1})}{N^2 - \sum_{i=1}^{k}(x_{i+} X\, x_{+1})}$$

Appendix E. Marsh sediment fraction distributions

Comparison between model outputs and field observations using the roughness factor (**RF**) to determine marsh presence, and the vegetation algorithm (**VEG**).

		Mean Absolute Error (MAE)	Observations Standard Deviation Ratio (RSR)	Nash Sutcliffe Efficiency (NSE)	Willmott Modified Index of Agreement
		RF / VEG	RF / **VEG**	RF / **VEG**	RF / **VEG**
Carter Creek	Sand	0.08 / **0.08**	0.43 / **0.43**	0.81 / **0.82**	0.86 / **0.87**
	Mud	0.08 / **0.08**	0.43 / **0.43**	0.81 / **0.82**	0.86 / **0.87**
Taskinas Creek	Sand	0.1 / **0.1**	0.61 / **0.62**	0.62 /**0.62**	0.83 / **0.82**
	Mud	0.1/**0.1**	0.61/**0.62**	0.62 / **0.62**	0.83 /**0.82**

Where:

Mean Absolute Error (MAE)	$\mathbf{MAE} = \frac{\mathbf{1}}{\boldsymbol{n}} \sum_{\mathbf{i=1}}^{\mathbf{n}} \lvert \boldsymbol{P_i} - \boldsymbol{O_i} \rvert$
Willmott Modified Index of Agreement (dr)	$d_r = \begin{cases} 1 - \frac{\sum_{i=1}^{n} \lvert P_i - O_i \rvert}{c \sum_{i=1}^{n} \lvert O_i - \bar{O} \rvert}, \ when \\ \sum_{i=0}^{n} \lvert P_i - O_i \rvert \leq c \sum_{i=0}^{n} \lvert O_i - \bar{O} \rvert \\ \frac{c \sum_{i=1}^{n} \lvert O_i - \bar{O} \rvert}{\sum_{i=1}^{n} \lvert P_i - O_i \rvert} - 1, when \\ \sum_{i=0}^{n} \lvert P_i - O_i \rvert > c \sum_{i=0}^{n} \lvert O_i - \bar{O} \rvert \end{cases}$ c=2
Nash_Sutcliffe Efficiency (NSE)	$\mathrm{NSE} = 1 - \frac{\sum_{i=1}^{n} (O_i - P_i)^2}{\sum_{i=1}^{n} (O_i - \bar{O})^2}$
Observations Standard Deviation Ratio (RSR)	$RSR = \frac{RMSE}{STDEV_{obs}} = \frac{\left[\sqrt{\sum_{i=1}^{n} (O_i - P_i)^2}\right]}{\left[\sqrt{\sum_{i=0}^{n} (O_i - \bar{O})^2}\right]}$

Appendix F. Interpretation of the model performance measures – Levels of agreements.

	Less than chance agreement	Slight agreement	Fair agreement	Moderate agreement	Substantial agreement	Almost perfect agreement
Kappa Statistic [1]	<0	0.01-0.20	0.21-0.40	0.41-0.60	0.61-0.80	0.81-0.99

	Unsatisfactory	Satisfactory	Good	Very Good
NSE [2]	< 0.50	0.50 < NSE < 0.65	0.65 < NSE < 0.75	0.75 < NSE < 1.0
RSR[3]	> 0.70	0.60 < RSR < 0.70	0.50 < RSR < 0.60	0.00 < RSR < 0.50

	Possible values	Optimal value	Preferred values
MAE [4]	0 to ∞	0	Low values
Willmott index of agreement [4 5]	0 to 1	1	0.5 to 1.0 [6] > 0.8 [7]

Based on: [1]Viera and Garret, 2005; [2]Moriasi et al. 2007; [3]Singh et al. 2004; [4]Bennett et al.2013; [5]Willmott et al. 2012; [6]Machiwal and Jha 2015; [7]De Jager 1994.

Appendix G – Change in Elevation of the Marsh Platform

Table G.1 Change in elevation of the marsh platform computed at each sampled point in **Carter Creek** using the **TMM_RF**. The dominant process is identified in each point along the transects (i.e., high marsh = H; medium marsh = M, and low marsh = L).

ID (Marsh Cores)	Elevation Change in 40 yrs (mm)	Elevation Change per year (mm/yr)	Location of the core	Dominant Process
1	0.0	0.0	L	no change
2	0.0	0.0	M	no change
3	0.0	0.0	H	no change
4	0.0	0.0	L	no change
5	0.0	0.0	M	no change
6	0.0	0.0	H	no change
7	-1131.8	-28.3	L	erosion
8	4.2	0.1	M	deposition
9	0.7	0.0	H	deposition
10	-134.1	-3.4	L	erosion
11	-861.5	-21.5	M	erosion
12	-710.7	-17.8	H	erosion
13	-832.8	-20.8	L	erosion
14	-300.4	-7.5	M	erosion
15	-687.3	-17.2	H	erosion
16	-253.4	-6.3	L	erosion
17	-223.0	-5.6	M	erosion
18	-529.9	-13.2	H	erosion
19	-106.9	-2.7	L	erosion
20	20.2	0.5	M	deposition
21	0.0	0.0	H	no change
22	149.8	3.7	L	deposition
23	0.0	0.0	M	no change
24	0.0	0.0	H	no change
25	0.0	0.0	L	no change
26	0.0	0.0	M	no change
27	0.0	0.0	H	no change
28	-776.1	-19.4	L	erosion
29	-5.0	-0.1	M	erosion
30	-118.8	-3.0	H	erosion
31	234.7	5.9	L	deposition
32	-0.2	0.0	M	erosion
33	0.0	0.0	H	no change

Table G.2 Change in elevation of the marsh platform computed at each sampled point in **Carter Creek** using the **TMM_VEG**. The dominant process is identified in each point along the transects (i.e., high marsh = H; medium marsh = M, and low marsh = L).

ID (Marsh Cores)	Elevation Change in 40 yrs (mm)	Elevation Change per year (mm/yr)	Location of the core	Dominant Process
1	0.0	0.0	L	no change
2	0.0	0.0	M	no change
3	0.0	0.0	H	no change
4	0.0	0.0	L	no change
5	0.0	0.0	M	no change
6	0.0	0.0	H	no change
7	-418.5	-10.5	L	erosion
8	4.4	0.1	M	deposition
9	-4.3	-0.1	H	erosion
10	-23.5	-0.6	L	erosion
11	-611.1	-15.3	M	erosion
12	-603.1	-15.1	H	erosion
13	-313.3	-7.8	L	erosion
14	-258.0	-6.4	M	erosion
15	-552.6	-13.8	H	erosion
16	-175.6	-4.4	L	erosion
17	-110.3	-2.8	M	erosion
18	-170.5	-4.3	H	erosion
19	-41.1	-1.0	L	erosion
20	-2.1	-0.1	M	erosion
21	0.0	0.0	H	no change
22	119.2	3.0	L	deposition
23	0.0	0.0	M	no change
24	0.0	0.0	H	no change
25	0.0	0.0	L	no change
26	0.0	0.0	M	no change
27	0.0	0.0	H	no change
28	-255.6	-6.4	L	erosion
29	-6.2	-0.2	M	erosion
30	-74.4	-1.9	H	erosion
31	238.6	6.0	L	deposition
32	-0.1	0.0	M	no change
33	0.0	0.0	H	no change

Table G.3 Change in elevation of the marsh platform computed at each sampled point in **Taskinas Creek** using the **TMM_RF** simulations. The dominant process is identified in each point along the transects (i.e., high marsh = H; medium marsh = M, and low marsh = L).

ID (Marsh Cores)	Elevation Change in 40 yrs (mm)	Elevation Change per year (mm/yr)	Location of the core	Dominant Process
1	-5.4	-0.1	L	erosion
2	-5.2	-0.1	M	erosion
3	17.3	0.4	H	deposition
4	0.0	0.0	L	no change
5	0.0	0.0	M	no change
6	0.0	0.0	H	no change
7	0.0	0.0	L	no change
8	0.0	0.0	M	no change
9	0.0	0.0	H	no change
10	492.2	12.3	L	deposition
11	0.0	0.0	M	no change
12	0.0	0.0	H	no change
13	305.0	7.6	L	deposition
14	177.0	4.4	M	deposition
15	0.0	0.0	H	no change
16	279.6	7.0	L	deposition
17	0.0	0.0	M	no change
18	0.0	0.0	H	no change
19	-387.5	-9.7	L	erosion
20	0.0	0.0	M	no change
21	104.6	2.6	H	deposition
22	-0.5	0.0	L	erosion
23	0.0	0.0	M	no change
24	0.0	0.0	H	no change
25	-559.9	-14.0	L	erosion
26	0.0	0.0	M	no change
27	0.0	0.0	H	no change

Table G.4 Change in elevation of the marsh platform computed at each sampled points in **Taskinas Creek** using the **TMM_VEG** simulation. The dominant process is identified in each point along the transects (i.e., high marsh = H; medium marsh = M, and low marsh = L).

ID (Marsh Cores)	Elevation Change in 40 yrs (mm)	Elevation Change per year (mm/yr)	Location of the core	Dominant Process
1	-1.9	0.0	L	erosion
2	-4.3	-0.1	M	erosion
3	6.9	0.2	H	deposition
4	0.0	0.0	L	no change
5	0.0	0.0	M	no change
6	0.0	0.0	H	no change
7	0.0	0.0	L	no change
8	0.0	0.0	M	no change
9	0.0	0.0	H	no change
10	608.7	15.2	L	deposition
11	0.0	0.0	M	no change
12	0.0	0.0	H	no change
13	157.2	3.9	L	deposition
14	68.0	1.7	M	deposition
15	0.0	0.0	H	no change
16	-460.2	-11.5	L	erosion
17	0.0	0.0	M	no change
18	0.0	0.0	H	no change
19	-432.3	-10.8	L	erosion
20	0.0	0.0	M	no change
21	112.6	2.8	H	deposition
22	0.1	0.0	L	deposition
23	0.0	0.0	M	no change
24	0.0	0.0	H	no change
25	-307.8	-7.7	L	erosion
26	0.0	0.0	M	no change
27	0.0	0.0	H	no change

FIGURES

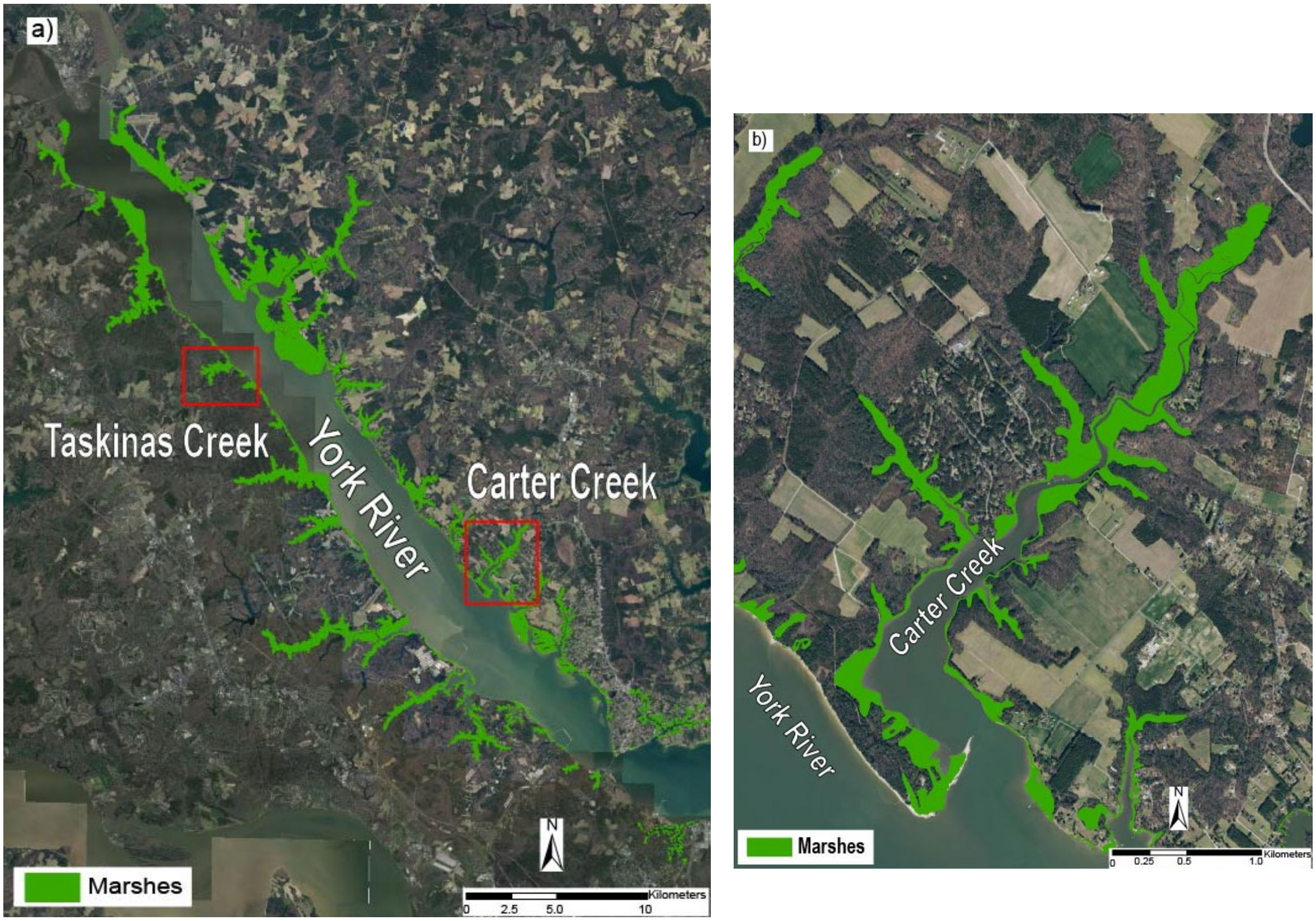

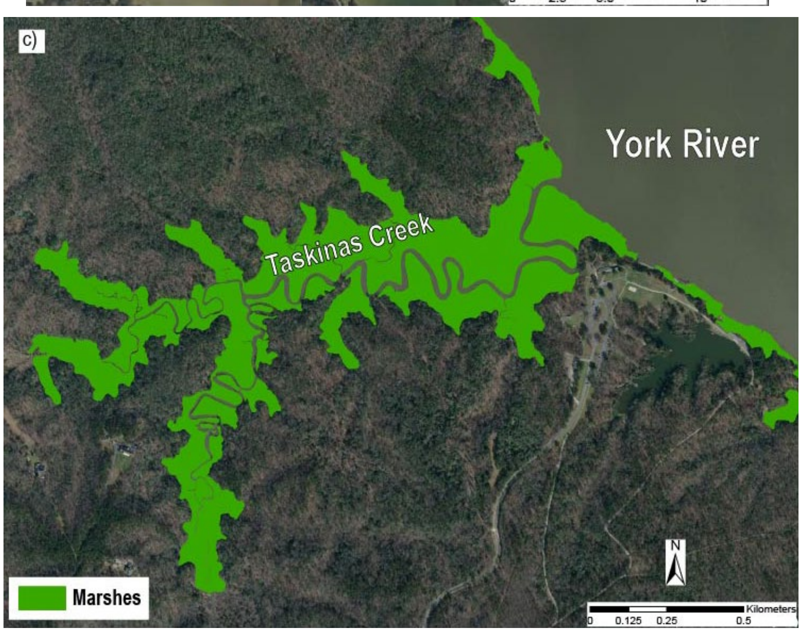

Fig. 1 a) York River system; b) Carter Creek and c) Taskinas Creek: study areas in the York River. Bright green areas represent tidal marshes. Background Image: VBMP2017/VBMP2017 WGS - Virginia Geographic Information Network (VGIN).

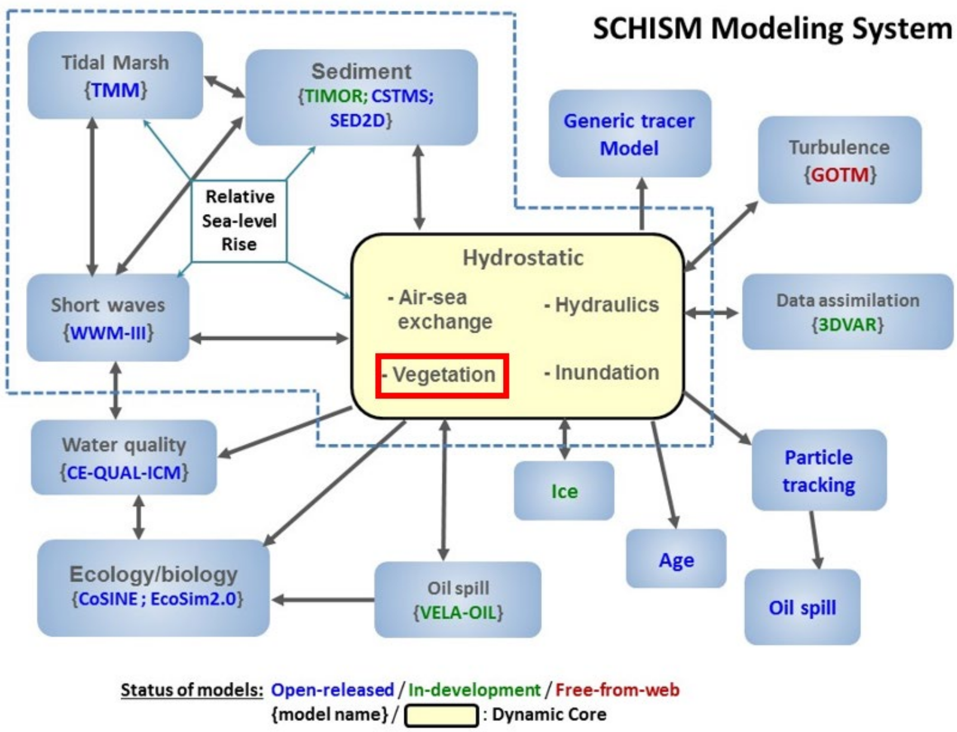

Fig. 2 SCHISM modeling system. The dashed box indicates key components of the TMM. The hydrostatic core serves as the pillar of the system to provide hydrodynamic variables to other models, as well as to facilitate exchange of variables between models in a parallel software environment

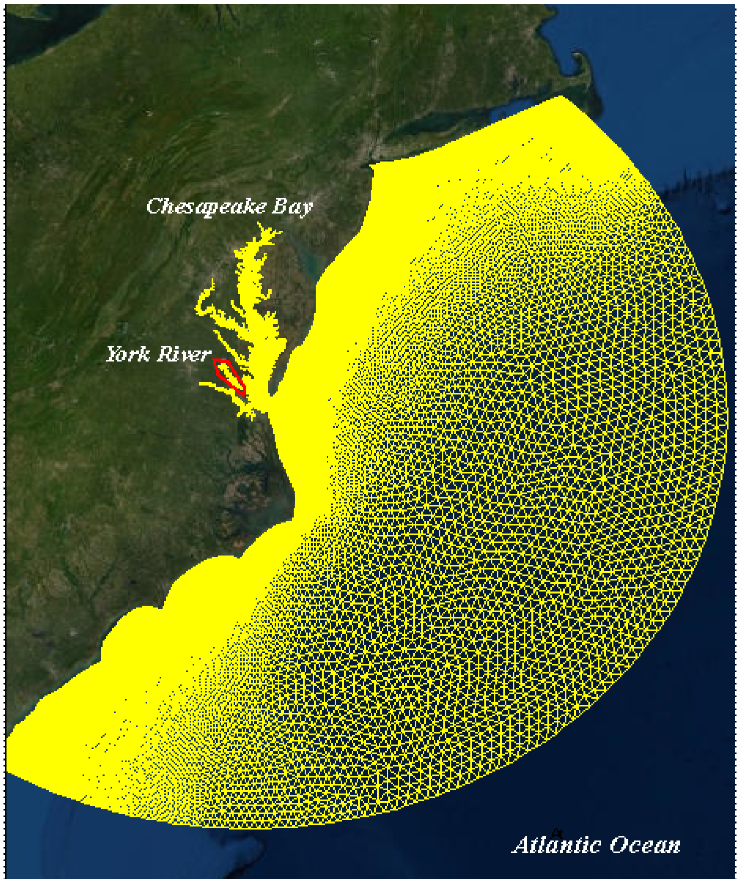

Fig. 3 Domain of the unstructured TMM_VEG grid used for the simulations in Carter Creek and Taskinas Creek. Background Image: ESRI world imagery

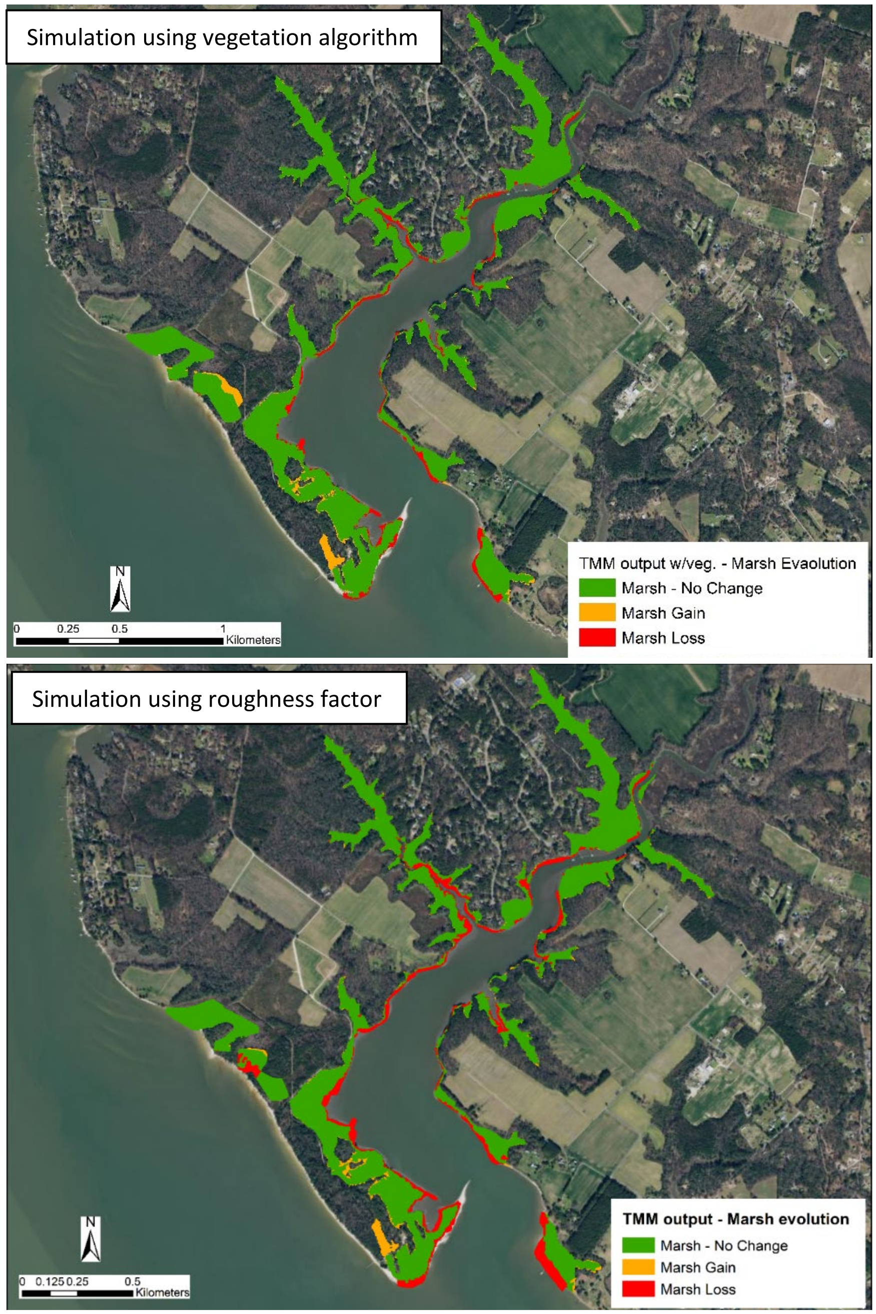

Fig. 4 Comparison of the marsh boundary evolution outputs for Carter Creek – Hindcast outputs: changes in marsh boundary after 40 years of simulation with a sea level rise of 4 mm/yr. Upper panel: **TMM_VEG**, Lower panel: **TMM_RF** simulations. Background image: VBMP2017/VBMP2017_WGS - Virginia Geographic Information Network (VGIN).

Fig. 5 Comparison of the marsh boundary evolution outputs for Taskinas Creek – Hindcast outputs: changes in marsh boundary after 40 years of simulation with a sea level rise of 4 mm/yr. Upper panel: **TMM_VEG**; Lower panel: **TMM_RF** simulations**.** Background image: VBMP2017/VBMP2017_WGS - Virginia Geographic Information Network (VGIN)

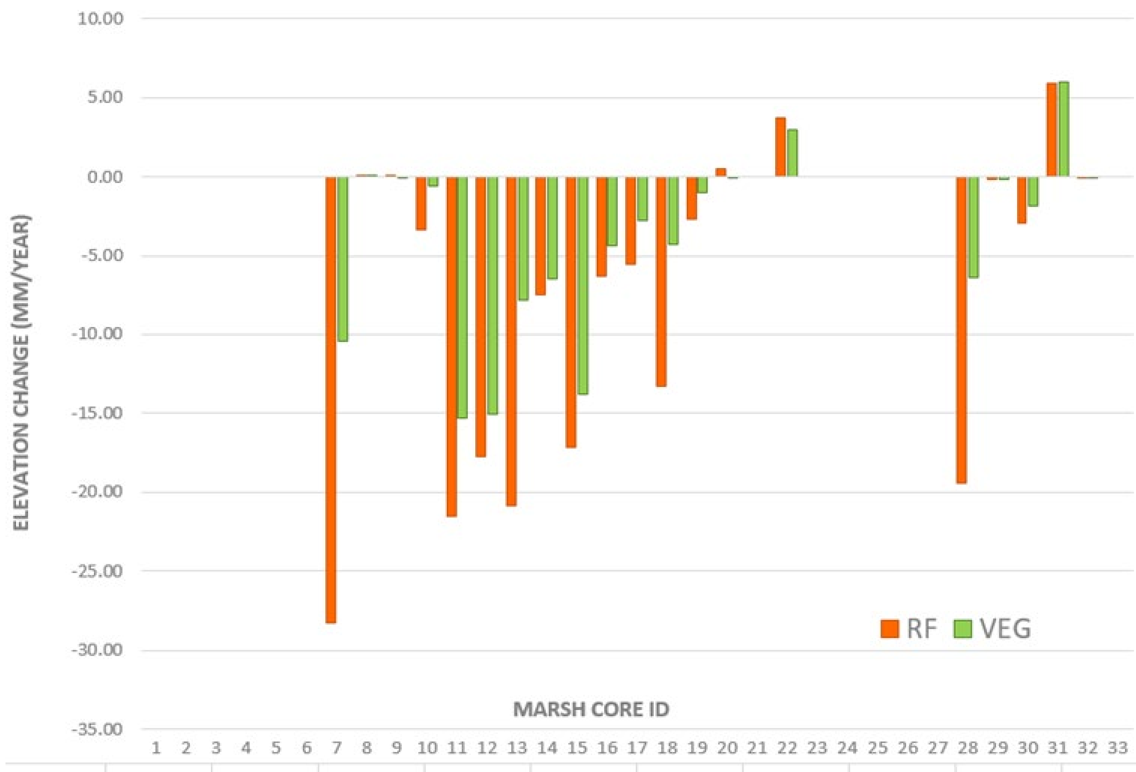

Fig. 6 Comparison of the changes in elevation of the marsh platform between the two simulations using the **roughness factor (RF)** and the **vegetation algorithm (VEG)** during the study period in Carter Creek. Positive numbers denote deposition, negative numbers correspond to erosion, and zero values indicate no change.

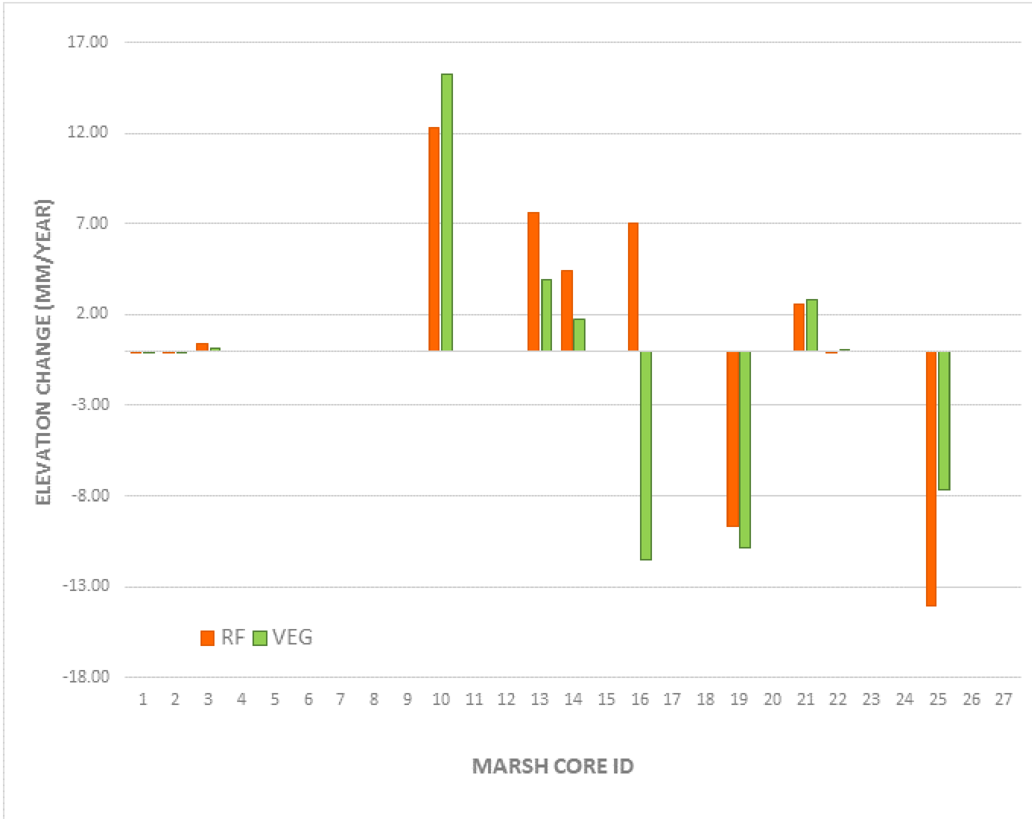

Fig. 7 Comparison of the changes in elevation of the marsh platform between the two simulations using the **roughness factor (RF)** and the **vegetation algorithm (VEG)** during the study period in Taskinas Creek. Positive numbers denote deposition, negative numbers correspond to erosion, and zero values indicate no change.

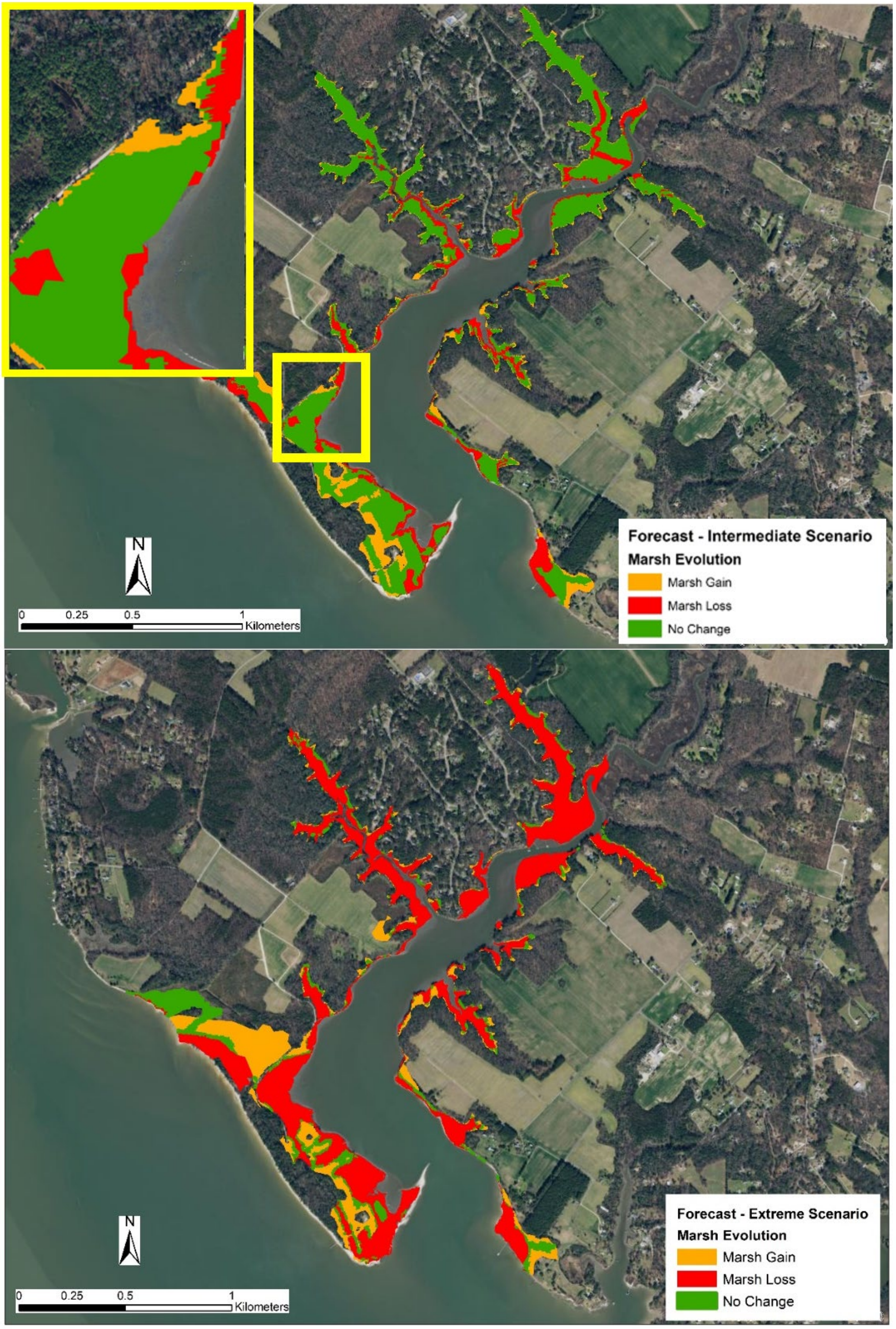

Fig. 8 Marsh boundary evolution output for Carter Creek. Forecast: 50-year simulation (2020-2070). Upper panel **intermediate SLR scenario** (an example of barriers for marsh landward migration is highlighted: presence of a road at the marsh-upland interface). Lower panel: **extreme SLR scenario.** Background image: VBMP2017/VBMP2017_WGS - Virginia Geographic Information Network (VGIN).

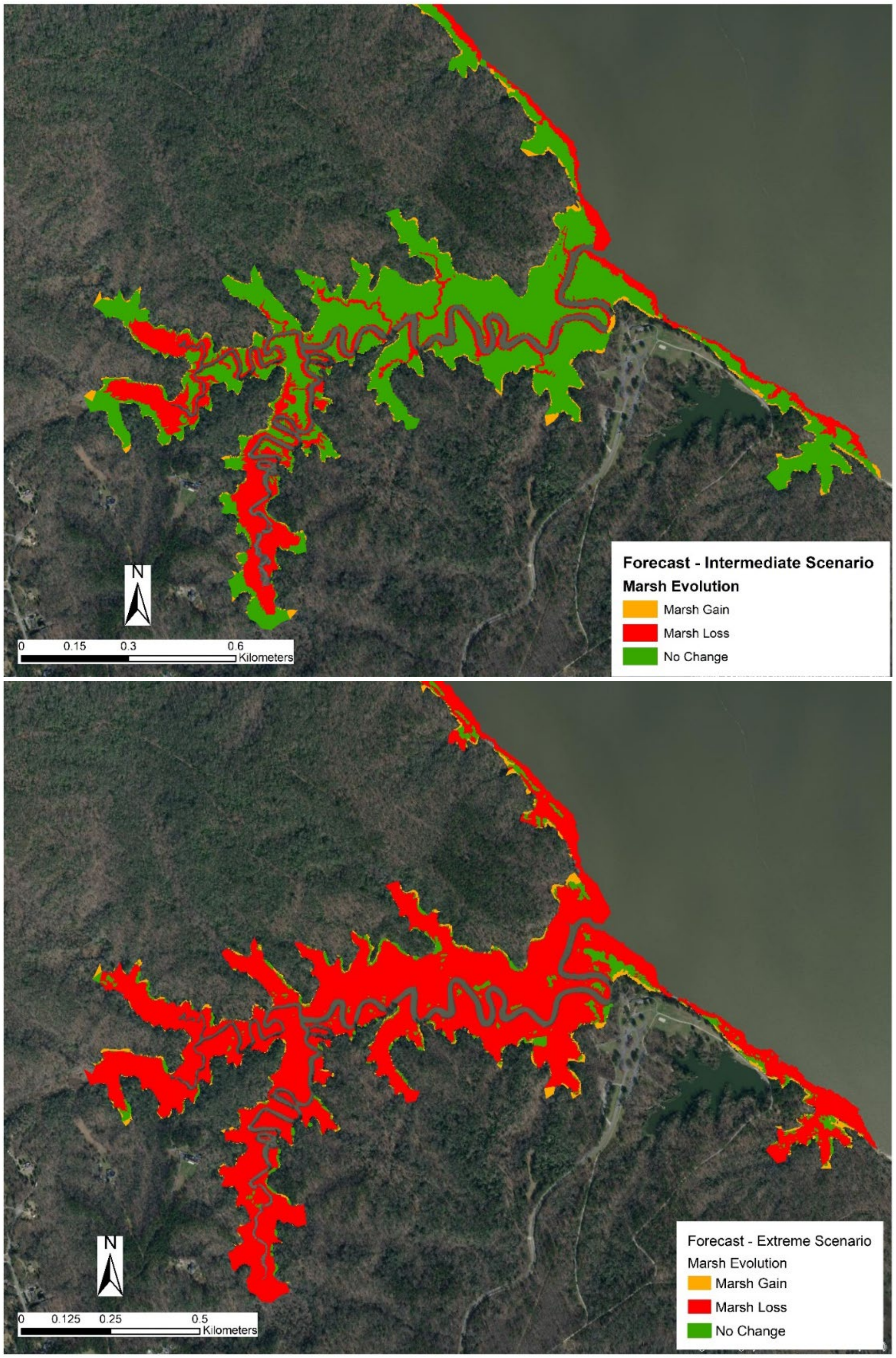

Fig. 9 Marsh boundary evolution output for Taskinas Creek. Forecast: 50-year simulation (2020-2070). Upper panel **intermediate SLR scenario**. Lower panel: **extreme SLR scenario.** Background image: VBMP2017/VBMP2017_WGS - Virginia Geographic Information Network (VGIN).